UNIVERSITEIT VAN PRETORIA
UNIVERSITY OF PRETORIA
YUNIBESITHI YA PRETORIA

Influence of a magnetic field on magnetic nanofluids for the purpose of enhancing natural convection heat transfer

by Johannes Joubert

Submitted in partial fulfilment of the requirements for the degree

MASTER OF ENGINEERING

in the Department of Mechanical and Aeronautical Engineering

University of Pretoria

February 2017

Abstract

Title: Influence of a magnetic field on magnetic nanofluids for the purpose of enhancing natural convection heat transfer

Supervisors: Prof Mohsen Sharifpur and Prof Josua Meyer

Department: Mechanical and Aeronautical Engineering

Degree: Master of Engineering (Mechanical Engineering)

Natural convection as a heat transfer mechanism plays a major role in the functioning of many heat transfer devices, such as heat exchangers, energy storage, thermal management and solar collectors. All of these have a large impact on the generation of solar power. Considering how common these devices are – not only in power generation cycles, but in a majority of other thermal uses – it is clear that increased performance for natural convection heat transfer will have consequences of a high impact. As such, the purpose of this study is to experimentally study the natural convection heat transfer behaviour of a relatively new class of fluids where nano-sized particles are mixed into a base fluid, also known as a nanofluids. Nanofluids have attracted widespread interest as a new heat transfer fluid due to the fact that the addition of nanoparticles considerably increases the thermophysical properties of the nanofluids when compared to those of the base fluid. Furthermore, if these nanoparticles show magnetic behaviour, huge increases in the thermal conductivity and viscosity of the nanofluid can be obtained if the fluid is exposed to a proper magnetic field. With this in mind, the study aimed to experimentally show the behaviour of these so-called magnetic nanofluids in natural convection heat transfer applications.

In this study, the natural convection heat transfer of a magnetic nanofluid in a differentially heated cavity is investigated with and without an applied external magnetic field. The effects of volume concentration and magnetic field configuration are investigated. Spherical Fe_2O_3 *nanoparticles with a diameter of 20 nm are used with a volume concentration ranging between 0.05% and 0.3%, tested for the case with no magnetic field, while only a volume concentration of 0.1% was used in the magnetic cases. The experiments were conducted for a range of Rayleigh numbers in* $1.7 \times 10^8 < Ra < 4.2 \times 10^8$*. The viscosity of the nanofluid was determined experimentally, while an empirical model from the literature was used to predict the thermal conductivity of the nanofluids. An empirical correlation for the viscosity was determined, and the stability of various nanofluids was investigated.*

Using heat transfer data obtained from the cavity, the average heat transfer coefficient, as well as the average Nusselt number for the nanofluids, is determined. It was found that a volume concentration of 0.05% showed an increase of 3.75% in heat transfer performance. For the magnetic field study, it was found that the best-performing magnetic field enhanced the heat transfer performance by 1.58% compared to the 0.1% volume concentration of the nanofluid with no magnetic field.

Keywords: *Nanofluid, natural convection, experimental, cavity, magnetic, Fe_2O_3, volume fraction*

Acknowledgements

I would like to thank my supervisors, Prof M. Sharifpur and Prof J.P. Meyer, for the guidance they offered throughout the duration of this study. I would also like to thank Dr A.B. Solomon for all the invaluable assistance and guidance provided during all the phases of the experimental and theoretical work done in this study, as well as Mr C. Govinder and Mr D.M. Keeste for all the help they provided during the reconstruction of the cavity. Finally, I would like to thank the University of Pretoria and the National Research Foundation for providing the facilities and funding needed to carry out this study.

Table of contents

List of figures

List of tables

Nomenclature

List of symbols

A	Area	m^2
c_p	Specific heat	$\mathrm{J/kg \cdot K}$
d	Diameter	m
g	Gravitational acceleration	$\mathrm{m/s}^2$
h	Heat transfer coefficient	$\mathrm{W/m}^2 \cdot \mathrm{K}$
H	Cavity height	m
k	Thermal conductivity	$\mathrm{W/m \cdot K}$
k_B	Boltzmann constant	$\mathrm{m}^2 \cdot \mathrm{kg/s}^2 \cdot \mathrm{K}$
L	Cavity length	m
L_c	Characteristic Length	m
m	Mass	kg
$\dot{m}$	Mass flow rate	$\mathrm{kg/s}$
P	Pressure	Pa
$\dot{q}$	Heat flux	$\mathrm{W/m}^2$
$\dot{Q}$	Heat transfer	W
r	Radius	m
T	Temperature	K
t_v	Nanolayer thickness	m
u	Velocity	$\mathrm{m/s}$
V	Volume	m^3

Dimensionless parameters

a	Correlation constant
b	Correlation constant
c	Correlation constant
Gr	Grashof number
k^*	Dimensionless thermal conductivity
Nu	Nusselt number
Pr	Prandtl number
Ra	Rayleigh number
T^*	Dimensionless temperature
ϕ	Volume fraction

Greek letters

ρ	Density	$\mathrm{kg/m^3}$
μ	Dynamic viscosity	$\mathrm{Pa \cdot s}$
ν	Kinematic viscosity	$\mathrm{m^2/s}$
β	Thermal expansion coefficient	$1/\mathrm{K}$

Subscripts

bf	Base fluid
c	Characteristic/cold
eff	Effective
f	Fluid
h	Hot
i	Inlet
nf	Nanofluid
o	Outlet
p	Particle
s	Surface
v	Nanolayer
0	Base/reference
∞	Free stream/bulk

Chapter 1: Introduction

With the ever-increasing need for more efficient means of power generation, it is vital to look at every possible means of improving the performance of power generation cycles. A potential area in which improvements to power cycles can be made is to consider the working fluid used. With nanofluids starting to show great promise as a new heat transfer fluid, along with the relative ease of incorporating these fluids into an already existing system, the applicability of nanofluids, not only to power generation cycles, but to all thermal transport systems, should be investigated.

Research into the use of nanofluids as a heat transfer fluid can also provide benefits when looking at cooling applications. A promising application of this idea would be the cooling of micro- and nano-electronics, as these systems are already suffering from the limited heat transfer capacities of conventional fluids.

The reason why nanofluids are considered a better heat transfer fluid when compared to conventional heat transfer fluids revolves around the increased thermal conductivity of the nanofluid. A possible way to increase the thermal conductivity of a fluid is to suspend particles in the fluid. Due to the high thermal conductivity of the particles, at least intuitively, it makes sense that this will increase the thermal conductivity of the fluid. The issue with this idea is that when large particles with diameters in the range of millimetres or micrometres are considered, the suspension of these particles in the fluid is found to be very unstable, and so the particles settle rapidly. The large particles may also cause abrasion or clogging in the heat transfer system [1].

Nanofluids are fluids that contain suspended solid nanoparticles. By using nanoparticles, the problems with rapid settlement, as well as incompatibility with a system, can be solved. Again, these nanofluids have been shown experimentally to have an increased thermal conductivity when compared to that of the base fluid [1]. Furthermore, it has been shown that when using magnetically conducting nanoparticles and exposing the magnetic nanofluid to an external magnetic field, the thermal conductivity can be enhanced by up to 300% of that of the base fluid. However, this enhancement is only in the direction of the magnetic field [2].

The addition of nanoparticles does not only increase the thermal conductivity of the fluid, but also its viscosity [3]. When considering that the increase in thermal conductivity allows for more efficient heat transfer, while the increased viscosity increases the work required to transport the nanofluid, these two properties are clearly working against each other. When considering the overall efficiency of the system, this suggests that an optimal working condition exists where the increase in efficiency is at a maximum. As with the thermal conductivity, a similar trend can be found for the viscosity of magnetic nanofluids in a magnetic field [4].

When considering the optimisation of a magnetic nanofluid in natural convection, a wide variety of parameters can be considered, including the properties defining the nanofluid, such as volume fraction, particle size and particle material.

The focus of this study will be specifically on investigating the effects of a stationary magnetic field on the heat transfer of a magnetic nanofluid in natural convection. This will be done by using experimental results obtained from a square-cavity natural-convection setup with and without an applied magnetic field. Since the bulk thermal properties are measured beforehand, a model can be

developed to determine the effects that the magnetic field has on the heat transfer. Models for viscosity will also be determined for cases with no applied magnetic field.

The thesis will continue with the remainder of this chapter being focused on defining the problem statement, as well as presenting the literature survey that was performed for this study.

Chapter 2 describes the experimental setup and method used to determine the effects of volume concentration, as well as the magnetic field on the heat transfer of a nanofluid in a square cavity driven by natural convection.

Chapter 3 presents the results of the characterisation process used to determine the nanofluid's thermophysical properties, as well as its stability. This is done by experimentally determining the viscosity and stability of the nanofluid, as well as presenting empirical models for the thermal conductivity of the tested nanofluids.

Chapter 4 presents the experimental results obtained from the heat transfer study with the purpose of determining the effects of volume concentration and applied magnetic fields on the heat transfer behaviour of the nanofluids.

As the final chapter, Chapter 5 will contain a summary of all the results presented in this work. Comments will also be made on possible improvements to this study, as well as future work that can follow from the findings of this study.

1.1 Problem statement

While the use of both magnetic and standard nanofluids as a heat transfer fluid in natural convection has been investigated numerically to a rather large extent, there is a lack of experimental data to support the results obtained. As a partial solution to this problem, the purpose of this study is to experimentally determine the effects of an applied magnetic field on a magnetic nanofluid in a square cavity driven by the effects of natural convection.

In order to study this effect, the following tasks will need to be done: preparation and characterisation of the magnetic nanofluid, construction of the experimental setup and testing of the nanofluids in various conditions.

The method used to prepare a suitable nanofluid for study will have to be determined. The most suitable method will be chosen by determining the stability of the nanofluid obtained by the process. The stability of the nanofluids will be determined by both visual inspection and measuring their thermophysical properties over an extended period of time.

Once the desired stability is obtained, the thermophysical properties of the nanofluid will be determined as a function of temperature in the range in which the nanofluids will operate. With this information, an empirical model will also be constructed. This will be done for all the nanofluids that will be used during the testing.

Finally, to obtain clear results of how different magnetic fields influence the heat transfer performance of the system, various cases will be considered. Among these cases are a run with only the base fluid to serve as a baseline for all other tests, a run for each nanofluid considered with no applied magnetic field, and various runs for different configurations of the applied magnetic field.

This allows for a comparison between the base fluid and magnetically excited nanofluid as well since the enhancement of heat transfer due to the addition of nanoparticles is also well established in this study.

1.2 Literature survey

This literature survey investigates three different areas: the various factors that influence the thermal conductivity and viscosity of a nanofluid, the behaviour of magnetic nanofluids in various magnetic field configurations, and the preparation of a stable nanofluid.

1.2.1 Thermal conductivity of nanofluids

From the literature, it is clear that the thermal conductivity of a nanofluid is a function of a wide variety of different variables. A review of different conductivity models developed by Aybar et al. [1] is summarised in this section.

Factors that influence the thermal conductivity of a nanofluid include the Brownian motion of the nanoparticles, the clustering of nanoparticles, the nanolayer of the liquid at the liquid/nanoparticle interface, the ballistic transport of non-local effects, thermophoretic effect and near-field radiation.

When considering the effects of the Brownian motion of the particles, two proposed methods can increase thermal conductivity. The first sees the particle as a carrier of heat, giving the thermal energy present in a warmer region more mobility, while the second takes into account the microconvection caused by the fluid moving around the particle. A number of thermal conductivity models are based on this idea. One thing that should be noted is that the more successful models do not only take account of the effects of Brownian motion, but rather contain correction factors or take other mechanisms into account, such as parallel heat transfer or the effects of particle agglomeration.

Another aspect to consider as a mechanism to increase the thermal conductivity of a nanofluid is the effects of the nanolayer around the nanoparticles. A nanolayer is a layer of fluid particles that forms around the nanoparticle and behaves like a solid layer. This can be seen as an intermediate physical state between the base fluid and the nanoparticle. Due to the small size of the nanolayer, it is likely that (as with the Brownian motion) this will not be the only dominant factor in the increase of the nanofluid's thermal conductivity.

The final mechanism that will be considered to increase the thermal conductivity of a nanofluid is the effect of nanoparticle clustering. Different researchers have observed the effects of clustering to have opposite effects on the thermal conductivity of the nanofluid. The reason for these two contradictory results revolves around the two different mechanisms that were present in both systems.

To explain the decrease in thermal conductivity, one needs to realise that, in an area with low nanoparticle density, the thermal conductivity is lower, since the thermal conductivity of the base fluid is lower than that of the nanoparticle. When clustering of nanoparticles occurs, the nanoparticles involved are much more prone to settle. With fewer particles suspended in the fluid, this mechanism creates particle-free zones, which result in a reduction in thermal conductivity.

The increase in thermal conductivity due to clustering can be explained by considering that this larger collection of particles creates paths of lower thermal resistance in the fluid, with the added benefit that the volume of these zones of high heat conductivity is larger than the volume fraction of the individual particles.

For many cases, researchers have observed similar trends for specific types of nanofluids, but when changing a parameter such as particle size, different trends or even contradictory results are obtained. While the abovementioned mechanisms to enhance thermal conduction are considered at this stage to have the largest influences on nanofluids, other properties (such as particle settling time and pH) can also influence thermal conductivity and cannot be excluded until their effects have been investigated in more detail. Furthermore, even experimental data for what is claimed to be the same operating conditions yields different results, clearly showing the sensitivity of nanofluid properties to the applied system.

1.2.2 Viscosity of nanofluids

Unlike the thermal conductivity of nanofluids, limited work has been done on their viscosity. Meyer et al. [3] compiled a list of theoretical, empirical and numerical models for the viscosity of a fluid with suspended particles. This list contains models proposed for larger micro-sized particles, as well as nano-sized particles. As in the case of thermal conductivity due to nanoscale effects that have a considerable influence on the fluid properties, the models developed for larger particles that are suspended in a fluid are not applicable. As in the case of thermal conductivity, a variety of influencing factors and their effects are summarised below.

The theoretical models developed for the viscosity of nanofluids take account of a wide range of variables, such as temperature, particle volume fraction and nanoparticle size. Some models consider the fluid to be a two-phase system where a creeping flow assumption around a spherical nanoparticle is used. While the theoretical models are based on expected mechanisms to increase the viscosity of the nanofluid, these models also contain tuning parameters specific to each fluid case.

When considering empirical models, many researchers have proposed a simple linear polynomial function of volume fraction, while ignoring the temperature of the fluid. However, this has been shown not to be the case when considering the empirical correlation provided by Vakili-Nezhaad and Dorany (in Meyer et al. [3]), and so a temperature-dependant term needs to be included. Some models are based on the model proposed by Einstein (in Meyer et al. [3]), namely $\mu_{eff} = \mu_0(1 + [\eta]\phi)$, with some modified or additional terms.

An effect to be aware of is that the addition of nanoparticles to a Newtonian fluid may create a non-Newtonian nanofluid. However, this is not always the case. Experiments conducted by Hernández Battez (in Meyer et al. [3]) showed that, at shear rates below $700s^{-1}$, ZnO and ZrO_2, nanoparticles suspended in a polyalphaolefin base fluid behaved as a Newtonian fluid, while at high shear rates between 10^6 and $10^7 s^{-1}$, the nanofluids exhibited shear thinning behaviour with various trends.

Nguyen (in Meyer et al. [3]) considered a fixed volume fraction with only the nanoparticle size changing, namely a diameter of 36 nm as opposed to a 47 nm $Al_2O_3 - H_2O$ nanofluid at 4% volume fraction. It was found that the viscosity of the particle with a 47 nm diameter was higher. This trend was observed by other researchers as well. However, the opposite result was found by several

researchers where smaller particles produce higher viscosities. This is explained when considering the interactions between the base fluid and the particles, as well as the interactions between the nanoparticles. The electroviscous effects in the nanofluid influence agglomeration and so directly influence the Brownian motion of the particles. For smaller nanoparticles, the total surface area of the nanoparticles increases and so both the fluid-particle and the particle-particle interaction increase, increasing the electroviscous effects and so increasing the total viscosity. When the larger particles provide an increase in viscosity, this may be caused by agglomeration between particles, which would also clearly increase the viscosity.

It has also been proposed that intrinsic viscosity is not a function of the particle shape, but rather a function of agglomeration and electroviscous effects, which clearly also influence the viscosity.

Many other relations have been proposed for different nanofluids, which all determine the effects of different properties on nanofluid viscosity. From the literature, it is seen that the following parameters influence the viscosity of nanofluids: temperature, volume fraction, shear rate, size of the nanoparticle, shape of the nanoparticles, pH and the electrical conductivity of the suspension, and the base fluid properties.

One final technique used to determine the fluid properties of nanofluids revolves around applying computational techniques to determine how these fluids respond. One such case was carried out by Rudyak and Krasnolutskii (in Meyer et al. [3]), where a molecular dynamics simulation was performed to model the interactions between the molecules of a nanoparticle and its base fluid. With this technique, taking into account the particle-molecule interaction, the research team simulated the viscosity of lithium-argon and aluminium-argon nanofluids.

Other techniques involve using artificial neural networks and training them with experimental data to create a prediction model capable of modelling the highly non-linear input-output systems such as those between the nanofluid's properties and all the influencing factors. In 2012, Mehrabi (in Meyer et al. [3]) successfully used this technique to develop four models for Al_2O_3, CuO, TiO_2 and SiO_2 nanoparticles with water as a base fluid to determine the viscosity of these nanofluids.

1.2.3 Specific heat capacity of nanofluids

O'Hanley et al. [5] conducted an experimental comparison to obtain data using two models to predict the specific heat capacities of a nanofluid. The first model was based on a simple volume fraction estimation, while the second was based on the assumption of thermal equilibrium between the nanoparticle and the surrounding fluid.

The volume fraction model was given as:

$$c_{p,nf} = \phi c_{p,n} + (1-\phi)c_{p,f} \tag{1.1}$$

and the thermal equilibrium model was given as:

$$c_{p,nf} = \frac{\phi(\rho c_p)_n + (1-\phi)(\rho c_p)_f}{\phi\rho_n + (1-\phi)\rho_f} \tag{1.2}$$

This study found that the model based on the mixed volume fraction method (Equation 1.1) does not accurately predict the specific heat capacity of the nanofluid. However, the thermal equilibrium model was much more effective in predicting the specific heat capacity of the nanofluids.

The nanoparticle concentration of the tested nanofluids varied from 5 weight percentage to 50 weight percentage. All tested nanofluids were water-based with silica, alumina or copper oxide nanoparticles mixed with the water. For the whole range of tested nanofluids, the model was found to agree with the results determined experimentally.

1.2.4 Density of nanofluids

A common way of determining the density of a nanofluid is to use the combined mass of the base fluid and the dispersed nanoparticles and divide it by the combined volume of the two. A recent study by Sharifpur et al. [6] has shown this model to overestimate the density of the nanofluid, as it does not take into account the nanolayer that forms around the nanoparticle. It was found that the effect of the nanolayer on the density is greater for higher volume fractions.

In the model proposed, it is assumed that the nanolayer involves some void and so the density of the nanofluid is given as:

$$\rho_{nf} = \frac{m_p + m_f}{V_p + V_f + V_v} \tag{1.3}$$

Where m_p and m_f are the particle and fluid mass respectively, and V_p, V_f and V_v are the particle, fluid and void volumes respectively. It was found that the equivalent nanolayer thickness as pure void is a function of particle size and can be approximated as:

$$t_v = -0.0002833 r_p^2 + 0.0475 r_p - 0.1417 \tag{1.4}$$

Writing Equation 1.3 in terms of t_v gives the following:

$$\rho_{nf} = \frac{m_p + m_f}{V_f + V_p\left(r_p + t_v\right)^3 / r_p^3} \tag{1.5}$$

A detailed derivation is given in Sharifpur et al. [6]. This model was shown to be in agreement with the experimental results. However, it was also found that the standard volume fraction method gives acceptable results for volume fractions less than or equal to 1%.

The nanoparticles used in the experiments were SiO_2, SiOx, CuO and MgO with sizes ranging from 20 nm to 80 nm. Water, glycerol and ethylene glycol (EG)-water solutions were used as base fluids. The volume concentrations used were in the range of 1% to 6%. The density was measured in a temperature range from 10 °C to 40 °C.

1.2.5 Effects of a magnetic field on the thermophysical properties of magnetic nanofluids

As mentioned above, it has been shown that adding magnetic nanoparticles to a base fluid can enhance the thermal conductivity of that base fluid considerably. Furthermore, when considering charged nanoparticles that respond to an external magnetic field, it has been seen that the magnetic field can be tuned to change the effective thermal conductivity and viscosity of the nanofluid.

Philip et al. [2] conducted an experiment to show the tunability of a magnetic nanofluid's thermal conductivity. They used hexadecane as a base fluid with Fe_3O_4 nanoparticles coated in oleic acid with a mean diameter of $6.7\ \mathrm{nm}$. Various nanofluids were tested from 0% to 7.1% volume fraction with no applied magnetic field, which showed a relatively small increase in thermal conductivity with an insignificant effect up to 2.6% volume fraction and a maximum of 23% increase in thermal conductivity at 7.1% volume fraction.

Applying a uniform magnetic field to a 2.6% volume fraction nanofluid showed results as high as 128% at a field strength of $94.5\ \mathrm{G}$ with similar results for a 4.5% volume fraction (216% increase at $101\ \mathrm{G}$). It should be noted, however, that for a magnetic field below $20\ \mathrm{G}$, there is an insignificant increase in thermal conductivity. It was also shown that when the magnetic field is removed, the fluid would return to its original state, but following a slightly different path.

The reason for the slight hysteresis during the relaxation of the magnetic field is due to the fact that the nanoparticles are aligned in a more structured form, allowing the parallel heat conduction mode that drastically increases the thermal conductivity. This implies that these particles will first need to relax and resume the more randomly spaced patterns observed in a standard nanofluid before they perform in a manner similar to the original nanofluid. The two ways in which the nanoparticle structures formed by the magnetic field can relax are due to either Neel rotation or Brownian motion, which for individual nanoparticles of the size 10 nm are in the order of $10^{-9}s$ and $10^{-7}s$ respectively. Due to the relaxation time of Neel rotation being exponentially dependant on the size of the nanoparticles, this value can, however, be considerably higher. In this study, the measurement time of the thermal conductivity required 30 seconds, which should be far above the relaxation time for the nanoparticles. This shows that the relaxation time of these nanoparticles is much higher due to these particles forming a cluster. It was also noted that the maximum thermal conductivity of these nanofluids was very near the upper Hashin-Shtrikman limit. Finally, the reason for the maximum limit for thermal conductivity enhancement is based on the idea that as the chains responsible for the tremendous increase in thermal conductivity become too long, a zippering phenomenon takes place, breaking these chains and reducing thermal conductivity.

Shima et al. [4] showed that both the viscosity and thermal conductivity are tunable. It was shown that when taking a Fe_3O_4-kerosene nanofluid with a 0.078% volume fraction, it is possible to tune the thermal conductivity to viscosity ratio from anywhere between 0.725 and 2.35 by altering the magnetic field applied. In this study, it was noted that the fluid behaves like a Newtonian fluid over a range of shear rates for 100 to $1\,000\mathrm{s}^{-1}$. However, when agglomerates are formed, the fluid can show either shear thickening or shear thinning behaviour.

Magnetic fields with an intensity smaller than $100\ \mathrm{G}$ were found to have a rapid increase in thermal conductivity with respect to the applied field strength up to around 300% enhancement, while at the same time not effecting the viscosity to a noticeable degree. After that point, the thermal conductivity was found to start decreasing again until it reached a steady value of approximately 40% for any field strength after $400\ \mathrm{G}$. After $100\ \mathrm{G}$, the viscosity was also seen to increase with the magnetic field. It was suggested that this is due to the nanoparticles aligning in the fluid along the magnetic lines, allowing for a parallel mode conduction. Clearly, this also implies that the fluid properties become highly anisotropic, depending on the direction of the magnetic field.

This study also showed that, under the influence of any magnetic field, there was no enhancement in thermal conductivity at a volume fraction of 0.0011%. For a lower volume fraction up to 0.0057%,

very little enhancement was found in the viscosity, while the conductivity of the fluid was found to still be enhanced by approximately 50%, showing that this type of nanofluid is potentially a good candidate for heat transfer applications.

Li et al. [7] found similar results to Shima et al. [4]. Using a $Fe_3O_4 - H_2O$ nanofluid between 0.94% and 2.83% volume fraction with a particle diameter of 26 nm, the viscosity was found to increase by more than 240% at a maximum of $200\ \mathrm{G}$. See Table 2 for a comparison between these and the previous results, as well as results obtained by other groups.

Alsaady et al. [8] looked at a variety of studies from different research groups. One of the important findings of this study was that an increase in the thermal conductivity of the nanofluid is not strongly dependant on the thermal conductivity of the particle, as can be seen when comparing Fe_3O_4 nanofluids that outperformed other oxide-based nanofluids of the same volume fraction, such as Al_2O_3, CuO and TiO_2, even though the bulk thermal conductivity of Fe_3O_4 is less than that of the others.

In the presence of a magnetic field, both Philip et al. [2] and Gavili (in Alsaady et al. [8]), found an increase in thermal conductivity of 300% and 200% respectively. This increase in thermal conductivity was attributed to a chainlike structure forming in the direction of the magnetic field.

A wide range of similar studies was noted. The results can be found in Table 1, alongside other study results not mentioned by Alsaady et al. [8].

The viscosity of magnetic nanofluids was also considered in this study. It was suggested that the chainlike structures that cause the tremendous increase in heat transfer are also responsible for the increase in viscosity as these structures tend to block fluid motion. It is not surprising that the increase in viscosity is affected by the direction of the magnetic field. Patel et al. [27] showed that the viscosity of a magnetic nanofluid can increase by as much as 200% when the magnetic field orientation is changed from perpendicular to parallel with the flow direction. This study also showed that the stronger the magnetic field, the higher the viscosity. It is also suggested that, at low shear rates, the magnetic torques travelling through the suspension try to align the particles, but as the shear rate increases, this is less effective, and so shear thinning is observed.

Finally, to consider a case where the effective heat transfer of a heat transfer system is successfully increased, consider the study conducted by Goharkhah et al. [9], where the team looked into the effects of stationary and oscillatory magnetic fields on a magnetic nanofluid used in forced convection in a cylindrical pipe. The influences of the magnetic field strength, nanoparticle volume fraction and Reynolds number of the flow were taken into account. The study was conducted between $Re = 400 - 1200$ with a water-based magnetite ($Fe_3O_4 - H_2O$) nanofluid with a mean particle size of $30\ \mathrm{nm}$ and volume fractions of $\varphi = 1\%, 1.5\%$ and 2%. Three magnetic field intensities were used for both the alternating and stationary magnetic fields: $0\ \mathrm{G}, 300\ \mathrm{G}$ and $500\ \mathrm{G}$.

The experimental setup consisted of a pipe with four electromagnets placed in a staggered configuration alternating between the two sides of the pipe. The magnetic flux field for this configuration was found to be non-uniform across the entire length of the pipe. Using numerical simulations, the force on the magnetic nanoparticles was obtained. Hydrodynamic and gravitational forces on the nanoparticles were found to be of a much smaller order than that of the magnetic force, and so they were neglected in the study. The nanoparticles are also expected to be attracted

to the pipe surface due to the predicted forces being much larger in the direction from the pipe centre towards the magnets that are located outside.

The thermal conductivity and viscosity of all three nanofluids showed a similar behaviour to their base fluid with respect to temperature dependence, but an increase in the nanoparticles' volume fractions also leads to an increase in the ratio between the thermal conductivity and viscosity of the nanofluid and the base fluid.

The average heat transfer coefficient obtained for the case with no magnetic field at different flow rates was investigated. As expected from the trend observed with regard to thermal conductivity, the higher the nanoparticle volume fraction, the more effective the heat transfer characteristics of the fluid. Furthermore, for all ranges of tested flow rates, the improvements to the heat transfer were of the same order for each volume fraction tested.

The next set of tests carried out investigated the influence of alternating and static magnetic fields for the case of a nanofluid with a volume fraction of 1%. The alternating field was simply created by applying a rectangular signal to the electromagnet with a maximum voltage as desired to achieve the required magnetic field and a minimum of 0. This signal had a frequency of $f = 5\text{Hz}$. As can be seen from these results, the stronger the magnetic field, the higher the heat transfer. Of course, by only using two magnetic field strengths, it is not possible to predict at which magnetic field strength (if any) the effects of the magnetic field actually starts to negatively influence the heat transfer as it did with the thermal conductivity in the previous studies.

The reason for the increase in the heat transfer of this system is explained by considering how the nanoparticles move in this magnetic field. As mentioned previously, nanoparticles under the influence of a magnetic field tend to move towards the pipe surface. This shows that the nanoparticles will migrate to the surface, increasing the local thermal conductivity of the fluid. The particles will also be prone to form chain structures in the z-direction along the temperature gradient at the surface, allowing for parallel heat conduction modes at the surface. It has also been postulated that these nanoparticles at the surface can act as an obstruction to the flow, tripping the flow and causing turbulence, also increasing local heat transfer [9].

A possible reason for the alternating magnetic field having such a strong influence on the system is based on the idea that the nanoparticles themselves act as carriers of heat. In an alternating magnetic field, the particles that are located on the surface conduct heat at a very high rate, and when the magnetic field is turned off, these particles can move freely with the fluid. This process also disturbs the thermal boundary layer, increasing heat transfer.

The maximum heat transfer increase of 18.9% and 31.4% was found at a volume fraction of $\varphi = 2\%$ at a magnetic field strength of 500 G for the static and alternating magnetic field respectively.

1.2.6 Stability of magnetic nanofluids

Iron oxides are frequently used in magnetic nanofluids, so the stability of these nanofluids will be the focus of this section.

The first case that will be considered is the study of Zafarani-Moattar and Majdan-Cegincara [10]. In this study, the stability of a polyethylene glycol (PEG)-based nanofluid with Fe_3O_4 nanoparticles with an average size of 30 nm was investigated. The nanoparticles were treated with oleic acid and mixed with the PEG-based nanofluid using an ultrasonic mixer. It was found that the ratio between the oleic acid and PEG is important for the stability of the nanofluid. The ratios tested were 1:9, 3:7, 1:1, 7:3 and 9:1. It was found that a ratio of 1:9 was unstable, while the settling rate of the nanoparticles in the other nanofluids was determined using UV-Vis spectroscopy. From this, it was determined that the most stable nanofluid was the 1:1 oleic acid to PEG nanofluid.

A study by Yu et al. [11] considered a kerosene-based nanofluid with particles of Fe_3O_4 15 nm in diameter. In this study, the nanoparticles were treated with oleic acid. The stability of a 1% volume fraction Fe_3O_4-kerosene nanofluid was investigated over a period of six hours after synthesis. The stability of the nanofluid was determined by measuring the change in thermal conductivity over a five-hour period. The fluid was kept at a $30\ °C$ during the thermal conductivity measurements. It was found to be very stable with only a slight random variation, most likely due to measurement errors. This result inspires confidence in the stability of Fe_3O_4-kerosene nanofluids, especially at lower volume fractions.

A study by Hong et al. [12] considered a water-based Fe_3O_4 nanofluid with an average particle size of 10 nm. In this study, the nanoparticles were treated twice. The first treatment involved a process of coating the nanoparticles in sodium oleate, while the second was used to create a secondary layer of PEG-4000. The purpose of this two-stage treatment was to improve the stability of the nanofluid. The weight concentration and solid content of the tested fluid were 18.7% and 0.2 g/ml, respectively. The stability of the fluid was tested over a period of 60 days, and the results were found to be very promising.

The final case considered is that of Bateer et al. [13], where a bilayer is created around the nanoparticles to improve the stability of the nanofluid. A poly-alpha-olefin oil-based nanofluid with Fe_3O_4 particles was used in this study. The bilayer was created by first treating the Fe_3O_4 with oleic acid and then treating it with succinimide. In this study, it was found that the dispersibility of the nanoparticles was better for the coated nanoparticles than for the uncoated nanoparticles. It was also found that, at a constant room temperature, the nanofluid remained stable for 360 days.

1.2.6.1 Nanofluid stabilisers

Nanoparticles are still prone to rapid settlement for nanofluids with a higher volume fraction. A common method used to prevent this is to introduce a stabiliser into the nanofluid. In this section, the use of various stabilisers is investigated and compared.

In a study by Sun et al. [14], Al_2O_3, Fe_2O_3 and Cu-based nanofluids were investigated. The mass fractions ranged from 0.1% to 0.5%. Sodium dodecyl benzene sulfonate (SDBS) was used as a stabiliser for all three nanoparticles with the mass fractions of the SDBS ranging between 0.04% and 0.12% for 0.1 weight percentage for the nanoparticle case and 0.44% to 0.52% for the 0.5 weight percentage nanoparticle case. For every nanoparticle at every tested weight percentage, it was found that the optimum weight percentage of SDBS for maximum stability was close to the weight percentage of nanoparticles present in the fluid. For all case, the optimum was found to be at most ±0.02% from this value.

In another study that specifically looked at the stability of a Fe_2O_3-H_2O nanofluid, Sun et al. [15] investigated the use SDBS, gum acacia, and cetyl trimethyl ammonium chloride. The amount of stabilisers by mass percentage ranged between 0.00% and 0.14% increasing in intervals of 0.02% for a nanofluid with a 0.1% mass percentage Fe_2O_3. It was found that an increase in SDBS gradually increased the stability of the nanofluid up to a mass fraction of 0.1%, after which the nanofluid became increasingly less stable. A similar trend was observed with both the gum acacia and cetyl trimethyl ammonium chloride with optimal points at 0.08% and 0.1% weight percentage respectively. It was also found that, although all the stabilisers increased the stability of the nanofluid, SDBS has a much more drastic increase in the performance at all weight percentages when compared to the other two.

1.2.6.2 pH adjustment

The idea behind adjusting the pH of a nanofluid to increase its stability is based on the idea that a nanofluid with a pH equal or close to the isoelectric point (IEP), defined as the pH value at which a particular molecule carries no net electric charge, becomes unstable. The IEP is also the point at which the zeta potential is zero. Increasing the pH of the nanofluid therefore increases the hydration forces, allowing for a more stable fluid [16].

In a study by Li et al. [17], the effects of pH on the stability of a Cu-H_2O nanofluid were investigated. It was found that the pH of the nanofluid had a definite effect on its stability, with a pH of 9.5 showing good stability. The increase in stability was attributed to charge build-up on the surface of the Cu particles due to the addition of a stabiliser. In this study, $NaOH$ and HCl were used as a way of raising and lowering the pH of the nanofluid respectively.

Wen and Ding [18] investigated the effects of pH adjustment on TiO_2-H_2O nanofluids. The particle sizes used in this study were between 30 nm and 40 nm. However, due to agglomeration, the average particle size was found to be 170 nm. Dry particles were dispersed into the base fluid using an ultrasonic mixer, after which the fluid was processed in a high-shear homogeniser. The measured zeta potential for a 0.024% volume concentration nanofluid was presented as a function of pH. It was shown that the pH of the nanofluid has a drastic effect on its zeta potential. It was found that for pH values lower than 3, the zeta potential was close to $50\ mV$. It was also shown that the IEP (zeta potential of $0\ mV$) of this fluid was close to a pH of 6.5. For a pH larger than 8, the zeta potential was found to be in the range between -25 mV and -50 mV. The study chose to use a pH of 3. After several hours, a small amount of sedimentation was found. However, it was believed that these were agglomerates that were simply not broken down. Disregarding the initial sedimentation, the nanofluids were found to be stable for several weeks after preparation.

1.2.7 Natural convection heat transfer

In this section, a brief overview is given of important non-dimensional terms with regard to natural convection-dominated cases. Some empirical correlations for cavity flow driven by natural convection are also investigated. Experimental results for nanofluids driven by natural convection are also presented here.

1.2.7.1 Non-dimensional parameters

The driving force in natural convection is the buoyancy force term that is induced by changes in fluid density [19]. The coefficient of thermal expansion β of a fluid is used to express the variation of the fluid's density with variations in its temperature at a constant pressure. For small density variations:

$$\beta = \frac{1}{V}\left(\frac{\partial V}{\partial T}\right)_P = -\frac{1}{\rho}\left(\frac{\partial \rho}{\partial T}\right)_P \approx -\frac{1}{\rho}\left(\frac{\Delta \rho}{\Delta T}\right) = -\frac{1}{\rho}\left(\frac{\rho_\infty - \rho}{T_\infty - T}\right) \tag{1.6}$$

with ρ and T being the density and temperature of the fluid at a specific point respectively. The ∞ subscript indicates that the property of the fluid is far enough away from the wall to be considered unaffected by local effects. When considering a simple heated vertical plate, the pressure gradient caused by density variations can be expressed as $-\frac{\partial P}{\partial x} = g(\rho_\infty - \rho)$ with -x direction being the direction of gravity [19]. Clearly, the driving pressure for natural convection can be given as:

$$-\frac{\partial P}{\partial x} = g\beta(T - T_\infty). \tag{1.7}$$

This leads to a better understanding of the meaning of the Grashof number (Gr), given as:

$$Gr = \frac{g\beta(T_s - T_\infty)L^3}{\nu^2} \tag{1.8}$$

where g is the gravitational acceleration constant, T_s is the surface temperature, T_∞ is the bulk temperature, L is the length scale and ν is the kinematic viscosity. Looking at Equation 1.8, it can be seen that Gr is a measure of the ratio between buoyancy and viscous forces. Due to the driving forces of natural convective flow, it is not surprising that the range of Gr provides the main criterion in determining the flow regime present in the problem [19].

An important non-dimensional number for any heat transfer fluid is the Prandtl number (Pr), given as:

$$Pr = \frac{\nu}{\alpha} = \frac{c_P \mu}{k} \tag{1.9}$$

where α is the thermal diffusivity of the fluid, μ is the dynamic viscosity, c_p is the specific heat of the fluid and k is the thermal conductivity of the fluid. Considering the fluid properties that determine a fluid's Pr, it is clear why Pr is central to the performance of the heat transfer fluid, considering that it gives a measure of the ratio of the viscous diffusion rate to the thermal diffusion rate [19]. From this, it is also clear that a lower Pr is desired for heat transfer fluids in most applications.

The Nusselt number (Nu) plays a large role in any convection problems, considering that it can be seen as a non-dimensionalised heat transfer coefficient. Nu is given as:

$$Nu = \frac{hL}{k} \tag{1.10}$$

with h being the heat transfer coefficient. Heat transfer via pure conduction is proportional to k/L. For a case with convective heat transfer, the heat transfer rate is proportional to h. This implies that

Nu gives a measure of the enhancement of heat transfer due to convection with a larger Nu, implying a more effective convection system [19].

Finally, a non-dimensional number used frequently in natural convection problems is the Rayleigh number (Ra), given as:

$$Ra = GrPr \tag{1.11}$$

with Gr and Pr as defined in Equation 1.8 and Equation 1.9 respectively. The information contained in Ra can therefore be determined by looking at the information contained in Gr and Pr, so Ra can be seen as a measure of the ratio of buoyancy force with respect to the thermal and momentum diffusitivities. One of the reasons that Ra is important for natural convection applications is due to the strong relationship it has to Nu. As an example of this, for many natural convection cases, simple empirical correlations between Ra and Nu take the form of:

$$Nu = C(Ra)^n \tag{1.12}$$

with C and n being constants specific to the application [19].

1.2.7.2 Natural convection in a square cavity

Consider an enclosure with two opposite walls having isothermal conditions and all the other walls having adiabatic conditions. If all buoyancy effects are neglected, the dominating heat transfer effects would be due to pure conduction at sufficiently low temperatures of the hot and the cold walls. However, if the buoyancy effects are taken into account, the fluid would flow upwards at the hot wall and downwards at the cold wall, causing the fluid to flow from the hot to the cold wall of the cavity. Furthermore, when considering the form that the heat transfer rate takes through this cavity, the following analogy to a pure conduction case can be made:

$$\dot{q} = h(T_1 - T_2) = kNu(T_1 - T_2) = k_{eff}(T_1 - T_2) \tag{1.13}$$

with T_1 and T_2 being the temperatures of the hot and the cold walls respectively. This shows that heat transfer across a cavity behaves as an enhanced form of pure conduction if the system is considered in a global sense [19].

A simple relation proposed by Catton (1978) due to the results of Berkovsky and Polevikov (1977) between Nu and Ra for a rectangular cavity where the vertical walls have isothermal boundary conditions, as presented by Çengel and Ghajar [19], is given as:

$$Nu = 0.18\left(\frac{Pr}{0.2+Pr}Ra\right)^{0.29}, \quad \begin{matrix} 1 < H/L < 2 \\ PrRa/(0.2+Pr) > 10^3 \end{matrix} \tag{1.14}$$

$$Nu = 0.22\left(\frac{Pr}{0.2+Pr}Ra\right)^{0.28}\left(\frac{H}{L}\right)^{-1/4}, \quad \begin{matrix} 2 < H/L < 10 \\ Ra < 10^{10} \end{matrix} \tag{1.15}$$

where H is the height of the cavity and L is the length between the hot and the cold walls. Both Equation 1.14 and Equation 1.15 are applicable for any range of Pr.

1.2.7.3 Nanofluids in natural convection

While section 1.2.8.1 describes the natural convection heat transfer behaviour of a simple fluid, a nanofluid is not simply a new fluid with different thermophysical properties as it may seem at a glance. Nanofluids are effectively two-phase fluids with complex particle-fluid interactions. With this in mind, it is important to investigate the behaviour of nanofluids in natural convection as they may behave differently to that expected from a simple fluid with nanofluid thermophysical properties.

In a study by Wen and Ding [18], two heating plates were positioned horizontally in a tube with one placed above the other and the space between them filled with a nanofluid. The situation resembles a case where a hot plate is located at the bottom of a cavity and a cold plate at the top of the cavity. TiO_2-H_2O nanofluids with volume concentrations of 0.19%, 0.36%, and 0.57% were used in this study. It was found that the heat transfer decreases with an increase in volume concentration. This did not agree with numerical work for a similar case that considered nanofluids as incompressible Newtonian fluids with thermophysical properties similar to those of the nanofluid. Other experimental cases mentioned by Wen and Ding [18] showed similar results, specifically the differences present in nanofluids and simple single-phase fluids.

Moving on to a study similar to that presented in this dissertation, Ghodsinezhad et al. [20] investigated the natural convection heat transfer behaviour of Al_2-H_2O nanofluids by determining the behaviour of nanofluids in a differentially heated square cavity. In this study, the heat transfer performance was experimentally determined for nanofluids with a volume fraction between 0.0% and 0.6%. The particle diameter used was indicated to be 30 nm, but after investigation by a zetasizer, it was found that the average particle size in the nanofluid was in the range of 270 nm. The Ra of the test cases was kept in the range of $3.49 \times 10^8 \leq Ra \leq 1.05 \times 10^9$. It was found that, for a nanofluid with a 0.1% volume fraction, the heat transfer coefficient was enhanced by 15%. However, further increasing the volume fraction led to a decrease in performance. All nanofluids tested, however, showed an increase in heat transfer performance. The results of this study suggest that there is an optimum volume concentration that allows for maximum heat transfer enhancement.

1.2.8 Summary

In this section, the key ideas that naturally arise from the literature survey are summarised according to thermal conductivity, viscosity and stability.

1.2.8.1 Thermal conductivity

To first consider the increase in thermal conductivity in a general nanofluid, many different mechanisms have been proposed: Brownian motion of the particles that cause either micro-convection or act as a heat transfer mechanism, particle agglomeration and clustering as this increases the effecting particle size without increasing the volume fraction of the nanoparticles, parallel heat transfer modes through the fluid and particles, and enhanced heat transfer in the nanolayer [1]. With these different mechanisms come different models that have taken priority over certain mechanisms that are thought to dominate in specific situations. Accurate results have also been obtained through numerical simulations.

When considering the drastic improvement in thermal conductivity for magnetic nanofluids in a magnetic field, it has been proposed that the main mechanism responsible for this is the chainlike structure that forms in this fluid [4], [8] and [9]. It was found that, in the presence of a magnetic field, the nanoparticles will tend to align themselves along the direction of the magnetic field. These structures create parallel heat transfer paths inside the fluid, allowing for a massive increase in effective thermal conductivity. These chains are aligned along the direction of the magnetic field, clearly making the thermal conductivity anisotropic with the direction of maximum increase in thermal conductivity, lying parallel to the magnetic field. The strength of the magnetic field was found to increase the length of these chains, which in turn increases thermal conductivity, but after a certain length, these chains start to zipper, limiting the effectiveness of this phenomenon [2] and [4].

Table 1 provides a summary of the studies considered by Alsaady et al. [8]:

Table 1: Summary of the studies on enhancing thermal conductivity in magnetic nanofluids under different conditions as summarised by Alsaady et al. [8], unless stated otherwise

Researchers	Base fluid	Particle type	Average particle size (nm)	Volume fraction (%)	Enhancement with no magnetic field	Enhancement with magnetic field
Philip et al.	Kerosene	Fe_3O_4	6.7	0.03 to 7.8	23% at 7.8%	300% at 6.3% (80 G)
Gavali	Water	Fe_3O_4	10	5	–	200%
Parkeh and Lee	Kerosene	Fe_3O_4	10	1 to 10	17% at 4.7%, 38% at 10%	30% at 4.7%
Yu et al.	Kerosene	Fe_3O_4	15	0.1 to 1	34% at 1%	–
Li et al.	Water	Fe_3O_4	26	1 to 5	14% at 5%	13% at 1%, 44% at 5% (250 G)
Pastoriza-Gallego et al.	Ethylene glycol	Fe_2O_3	15	0 to 6.9	15% at 6.9%	–
Altan et al.	Water and heptane	Fe_3O_4	10	1 to 7	–	5.2% in water 2.8% in heptane at 2% (0.2 T)
Abareshi et al.	Water	Fe_3O_4	10	0.25 to 3	11.5% at 3%	–
Sundar et al.	Water	Fe_3O_4	13	0.2 to 2	25% at 2%	–
Nkurikiyimfura et al.	Engine oil	Fe_3O_4	10	0.01 to 0.05	–	200%
Shima et al. [4]	Kerosene	Fe_3O_4	2.5 to 10	0.0011 to 0.0171	–	300% at 0.078% (100 G)

Researchers	Base fluid	Particle type	Average particle size (nm)	Volume fraction (%)	Enhancement with no magnetic field	Enhancement with magnetic field
Karimi et al. [21]	Water	Fe_3O_4	10	0.25 to 4.8	12% at 4.8% (20 °C) 22% at 4.8% (60 °C)	143% at 4.8% (0.1235 T)
Karimi et al. [21]	Water	Fe_2O_3	10	0.25 to 4.8	14% at 4.8% (20 °C) 25% at 4.8% (60 °C)	20.3% at 4.8% (0.1235 T)
Azizian et al. [22]	Water	Fe_3O_4	60	0.86	–	167% (0.032 T)
Harandi et al. [23]	Ethylene glycol	MWCNT/ Fe_3O_4 Mixture	MWCNT: 5-15 inner 3-5 outer Fe_3O_4: 20-30	0.1 to 2.3	30% at 2.3% (50 °C)	–

It can be noticed that, while there is always an enhancement in thermal conductivity by dispersing nanoparticles into the fluid, all the magnetic nanofluids are enhanced even further in the presence of the magnetic field.

1.2.8.2 Viscosity

Unlike thermal conductivity, the viscosity of nanofluids is a much stronger function of the base fluid state and properties. Factors that influence the viscosity of nanofluids were seen to be temperature, nanoparticle volume fraction, shear rate, nanoparticle size and shape, the pH and electrical conductivity of the suspension, and the base fluid properties [3]. It should also be noted that the addition of nanoparticles can change the nanofluid from a Newtonian fluid to a non-Newtonian fluid at sufficiently high strain rates.

As in the case of thermal conductivity, for magnetic nanofluids, the increase in viscosity is larger when the fluid is exposed to a magnetic field. The mechanism responsible for this is similar to that of the increase in thermal conductivity. This is based on the idea that chainlike structures form in the fluid, and since these structures can block the flow locally, the effect of this on the bulk fluid can be seen as an increase in fluid viscosity. This leads to the viscosity also being anisotropic and, due to the same mechanism as in thermal conductivity that causes an increase in viscosity, the other mechanisms present, such as zippering, also affect viscosity [8].

Table 2 shows the results of different studies with respect to an increase in the viscosity of magnetic nanofluids. From these results, it can be seen that the shear rate plays a large role in the effective viscosity, since it is clear that magnetic nanofluids have shear thinning behaviour at sufficiently high shear rates. As discussed by Ghasemi et al. [24] and Odenbach and Störk [25], this is likely due to the destruction of the chainlike structures that are created by the magnetic field.

What can be noticed from the research of Shima et al. [4] is that even though the magnetic field increases the viscosity of the nanofluid, the enhancement to thermal conductivity relative to the

increase in viscosity is better in terms of the heat transfer application when the nanofluid is under the influence of a magnetic field.

Table 2: Summary of studies on an increase in the viscosity of magnetic nanofluids under different conditions

Researchers	Base fluid	Particle type	Average particle size (nm)	Volume fraction (%)	Increase with no magnetic field	Increase with magnetic field
Shima et al. [4]	Kerosene	Fe_3O_4	2.5 to 10	0.0011 to 0.0171	65% at 0.08%	180% at 0.0171% (500 G)
Li et al. [7]	Water	Fe_3O_4	26	0.94 to 2.83	–	240% at 2.83% (200 G)
Ghasemi et al. [24]	Kerosene	Fe_3O_4	10.6	–	–	450% at $137s^{-1}$ 150% at $1000s^{-1}$ (40 kA/m)
Odenbach and Störk [25]	–	Fe_3O_4	10	6.7	–	210% at $1.05s^{-1}$ 100% at $5.23s^{-1}$ (5 kA/m)
Sundar et al. [26]	Water	Fe_3O_4	13	0.3	27.85% at 20 °C 40% at 40 °C	–

From the research of Sundar et al. [26], it is clear that the temperature of the fluid also has a large effect on the viscosity of the nanofluid.

1.2.8.3 Stability

As seen in section 2.3.4, there is clearly a wide range of different cases that can be considered for a stable magnetic nanofluid. This being said, it is clear that it is likely that a treated nanoparticle will yield a much more stable nanofluid. As the results from literature suggest, it would be wise to, at the very least, treat the nanoparticles with oleic acid or to introduce a stabiliser such as SDBS.

While it was not explicitly tested in the other studies, it is clear that many studies have favoured kerosene as a base fluid due to the stable nature of the nanofluid. The reason for this being chosen as the base fluid in many studies revolves around how easy it is to create a fairly stable nanofluid. This is due to the fact that oleic acid as a Fe_3O_4 nanoparticles surfactant has a good compatibility with kerosene [11].

This shows that a good candidate would be a simple Fe_3O_4-kerosene nanofluid where the Fe_3O_4 particles are treated with oleic acid. However, it is also clear that iron oxide-water nanofluids can also show very good stability if a stabiliser is added.

Due to the applicability of water-based nanofluids, considering how common water is as a working fluid, not only for power generation applications, but also for general heat transfer systems, a water-based nanofluid will be used, and as such, an appropriate stabiliser will be used during preparation.

Chapter 2: Experimental details

In this chapter, the process used to prepare the Fe_2O_3-H_2O nanofluid is discussed. The configuration of the experimental setup is also discussed by describing how the differentially heated cavity is constructed and controlled, as well as discussing how the magnetic field is generated.

2.1 Nanofluid preparation

The preparation of the nanofluid used for the major part of this study was done in two stages. The first stage involved a mixing process where the nanoparticles were dispersed in deionised water, and agglomerates were broken down. A Hielscher UP200S ultrasonic mixer was used with the pulse time set to 60% and amplitude set to 65%. Sonication was carried out until all the nanoparticles were mixed into the fluid to obtain a homogeneous solution. Various samples were prepared with different sonication times, ranging from 20 to 80 minutes. Stability was observed visually. The sonication time of 40 minutes was found to be sufficient for a sample of 60 ml, with longer sonication times showing no noticeable benefit to the fluid stability.

The purpose of the second stage is to introduce and mix the stabiliser into the nanofluid. After the stabiliser has been added, the nanofluid is sonicated again. In this step, the fluid is only mixed for two minutes for the same 60 ml sample with the ultrasonic mixer using the same settings as before. The sonication time was again determined by a visual investigation of the stability of the nanofluid for mixing times between one and ten minutes. In a similar manner as in the previous experiment, no noticeable benefits were noticed for higher sonication times. The volume fraction of the nanofluid that was prepared in this manner ranged between 0.05% and 0.4%. The mass of the stabiliser added was the same as the mass of the nanoparticles. Sodium dodecyl sulphate (SDS) is used as a stabiliser for the nanofluid.

The nanofluids used in the natural convection experiments were prepared with a volume fraction between 0.05% and 0.3%. While it is true that the 0.4% volume fraction case was found to be stable, as seen in Chapter 3, the results presented in Chapter 4 show a steady decrease in performance from a volume concentration of 0.1% onwards. This inspired the study to rather ignore higher volume fractions for the time being and focus on the area in the range of 0.1%, since this is the point where substantial improvement to the heat transfer is found.

The nanofluid used in the pH study follows a similar procedure. The first step in preparing these nanofluids is exactly the same as in the stabiliser case. For the second step, no additional mixing is performed. Rather, the pH of the nanofluid is adjusted to a value of 9.5 using HCl and $NaOH$.

Spherical nanoparticles with a diameter of 15 to 20 nm, as specified by the manufacturer, were procured from US Nanomaterials Research, Inc. The size of nanoparticles was confirmed using TEM analysis with its results presented in chapter 3.3.

The mass of the nanoparticles to be introduced is determined as follows:

$$m_n = \left(\frac{\phi}{1-\phi}\right)\left(\frac{\rho_n}{\rho_{bf}}\right)m_{bf} \tag{2.1}$$

where m_n and m_{bf} are the mass of the nanoparticles and the base fluid respectively, ρ_n and ρ_{bf} are the density of the nanoparticle and the base fluid respectively, and ϕ is the desired volume fraction. The values of m_n, and m_{bf} are measured using a digital scale with a tolerance of 1 mg.

As discussed in Chapter 1, the density and the volume fraction of the nanofluid are not accurately described using this method. However, in order to apply and compare previous results to those found in this study, the older definition of nanofluid volume fraction is used.

2.2 Experimental configuration and procedure

To determine the response of a variety of nanofluids in natural convection, a differentially heated square cavity with dimensions of 99 x 96 x 120 mm (length x height x width) was constructed. Two opposite vertical walls are kept at a constant temperature, while all the other walls are insulated. The cavity is housed in the centre of a 650 x 650 x 650 mm wooden box with the void between the cavity and the box filled with insulation material.

The constant wall temperature boundary condition was created by using a copper shell and tube heat exchanger. In each heat exchanger, a copper plate that serves as the constant temperature wall of the cavity has three holes 2 mm in diameter drilled into it to allow the thermocouples to be placed inside the wall so that the temperature of the walls can be probed. They are isolated from the system and fixed in place using an epoxy to ensure accurate readings.

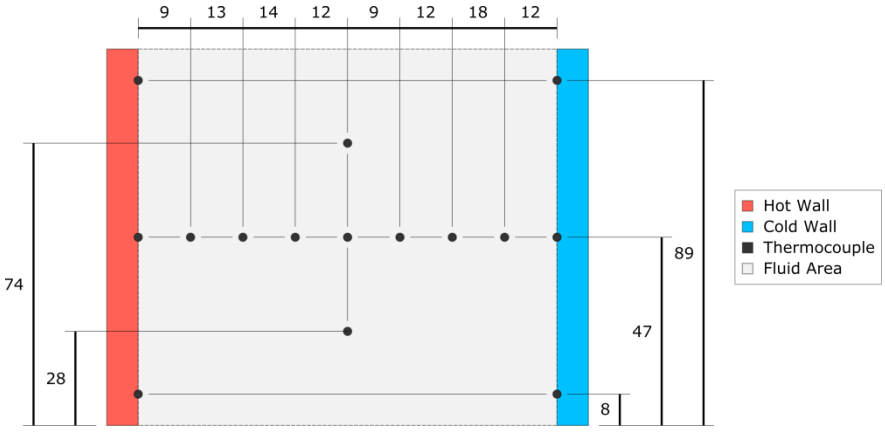

Figure 1: Thermocouple spacing inside the cavity with all measurements given in mm

To adjust and control the temperature of the hot and the cold walls, two PR20R-30 Polyscience constant thermal baths are connected to the heat exchangers. These thermal baths have a temperature range of -30 °C to 200 °C with an accuracy of 0.005 °C. Distilled water is used as the heat transfer fluid in the thermal bath/heat exchanger subsystem.

Four different temperature settings of both thermal baths were used to adjust the temperature of the hot and the cold walls. The hot wall's thermal bath was adjusted from 40 °C to 55 °C, while the cold side was adjusted from 20 °C to 5 °C with both changing in intervals of 5 °C. The mass flow rate is controlled via a series of valves that is adjusted until the heat flux at the cold side matches that of the hot side. Burkert type 8081 ultrasound flow meters were used to determine the volume flow rate. These flow meters can measure flow between the range of $0.06\ \mathrm{L/min}$ to $20\ \mathrm{L/min}$ with an accuracy of 0.01% of the full range base with an additional 2% of the measured value.

To determine the heat flux of both walls, thermocouples were mounted at the entrance and exit of the heat exchanger. Mixers were placed just before the thermocouples to break the boundary layer formation and ensure that the average fluid temperature is measured. Thermocouples were also placed inside the cavity to obtain readings of the fluid temperature inside the cavity. The spacing of the thermocouples can be seen in Figure 1. All thermocouples were calibrated using the thermal baths as a reference. All the thermocouples used were T-type thermocouples from Omega.

The flow meters, as well as the thermocouples, were connected to a data logger that was, in turn, monitored and recorded by a computer.

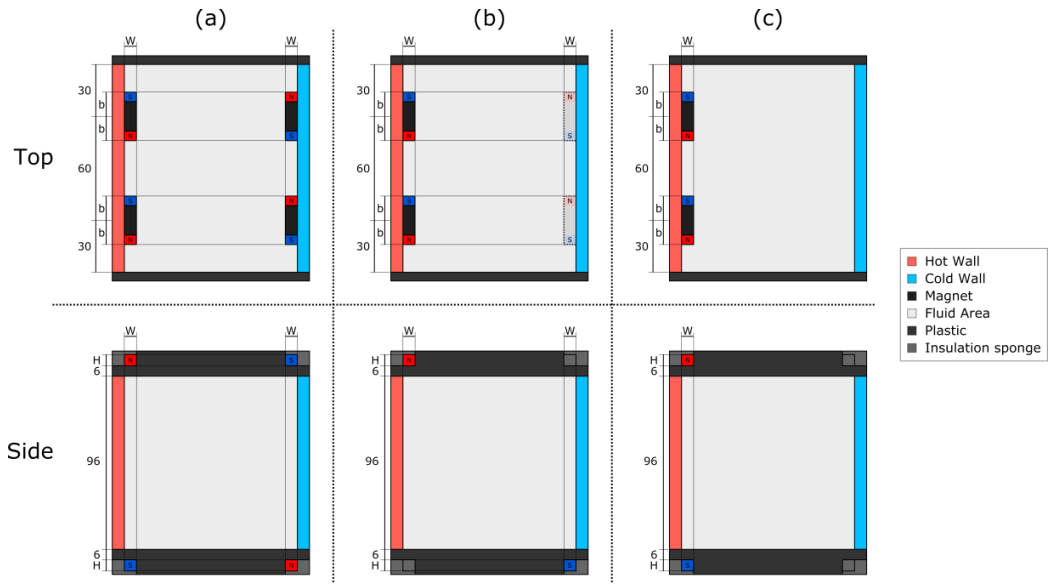

Figure 2: Configurations of permanent magnets used for exciting a magnetic nanofluid with: (a) four magnets located on the top and the bottom of the cavity; (b) two magnets located on the top of the hot wall and the bottom of the cold wall; and (c) two magnets located at the top and the bottom of the hot wall

Permanent magnets were used to generate a magnetic field. The magnets were housed in removable insulation material that fit neatly in the housing above and below the cavity. The three configurations of interest to this study can be seen in Figure 2.

The entire configuration was chosen as a way to generate magnetic field line in the direction of desired fluid flow thus increases the momentum of the nanoparticles. The focus of this study is on momentum excitation of the nanofluids and so no magnetic fields that inspire chainlike structure formation were explored. Configuration (a) was chosen as a way to saturate the whole cavity with a magnetic field with field lines moving with the expected fluid flow at the hot and cold wall. The downside to this configuration is that the magnetic field lines move in the opposite direction of the fluid along the insulated walls. It was desired to test configuration (b) for the possible case where near field magnetic effects dominate. Here it is expected that the magnetic field simply accelerates the nanoparticle only near the top of the hot wall and bottom of the cold wall while having a minimum effect on the flow in the rest of the cavity. Configuration (c) was chosen as a way to produce magnetic field line with the majority of the field along the direction of the hot wall only thereby mainly accelerating the nanoparticles along the hot wall. To investigate the effects of the magnetic field strength, all configurations were tested with two different magnets of varying magnetic field strengths.

Two different sets of eight anisotropic magnets were procured from Magnets4u.co.za. The catalogue code of the two magnets and respective geometries can be seen in Table 3, where the symbols are the same as those used in Figure 2. The surface magnetic flux is also provided.

Table 3: Magnet dimension and surface flux

	Height H (mm)	Width W (mm)	Length 2b (mm)	Surface magnetic flux (G)
MMA207	5	10	20	700
MMA210	10	15	50	300

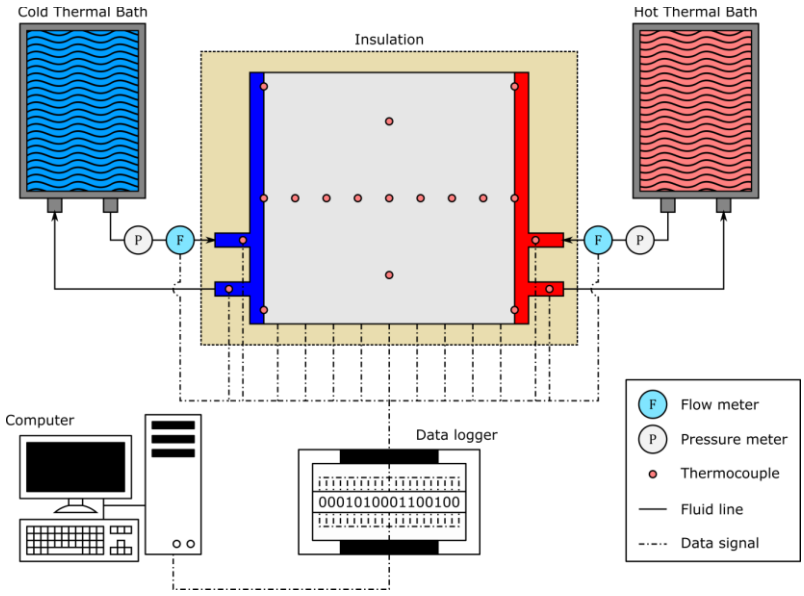

Figure 3: Schematic view of the experimental setup

Finally, a schematic view of the experimental setup can be seen in Figure 3. As indicated on the schematic overview, pressure sensors were also included in the system. However, these readings were not used in this study.

2.3 Analysis methodology

Once a steady-state condition is achieved and the results have been recorded, the heat transfer performance of the nanofluid is analysed by comparing the Nu at a similar Ra. In order to do this, the heat transfer coefficient and heat transfer need to be determined. Equation 2.2 is used to calculate the total heat transfer:

$$\dot{Q} = \dot{m} C_p \Delta T \tag{2.2}$$

where ΔT is the temperature difference over the heat exchanger. Since there are two thermocouples at the outlet, the temperature difference is calculated as:

$$\Delta T = \frac{\left(T_{o,1} + T_{o,2}\right)}{2} - T_i \tag{2.3}$$

where $T_{o,1}$ and $T_{o,2}$ are the two outlet temperature readings and T_i is the inlet temperature reading.

The following equation is used to determine the heat transfer coefficient:

$$h = \frac{\dot{Q}}{(T_h - T_c)A_s} \tag{2.4}$$

where A_s is the area of the heated wall, and T_h and T_c are the average wall temperatures of the hot and cold walls respectively.

Finally, the Nu is calculated as:

$$Nu = \frac{hL_c}{k} \tag{2.5}$$

where L_c is the characteristic length given as the distance between the hot and the cold wall (99 mm).

The analysis is carried out for both the hot and the cold wall.

The Ra will be calculated as given in Equation 1.11. As such, the Gr will also need to be calculated using the nanofluid's properties.

With the specific heat of a nanofluid defined by Equation 1.2 and the viscosity and thermal conductivity of the nanofluids defined later in Chapter 3, the only property still needed that has not yet been defined is the thermal expansion coefficient, which will be estimated as a weight average between that of the nanoparticle and the base fluid, also given as:

$$\beta_{nf} = \frac{(1-\phi)\beta_{bf}\rho_{bf} + \phi\beta_n\rho_n}{\rho_{nf}} \tag{2.6}$$

Chapter 3: Nanofluid characterisation and stability analysis

This chapter presents the results of the characterisation of the nanofluids by providing the viscosity obtained experimentally, as well as an empirical model used to estimate the thermal conductivity of the fluid. The results from the stability analysis of the nanofluids are also presented here.

3.1 Thermophysical properties

An SV-10 sine-wave vibro viscometer was used to measure the viscosity of the nanofluid over the temperature range from 15 °C to 60 °C. The viscometer was calibrated using deionised water at 15 °C. The measured viscosity of the nanofluids used during testing can be seen in Figure 4. From the results, it can be seen that the measurements of water are closer to the analytical curve at lower temperatures, with higher temperatures tending further away from the analytical curve.

A very definite trend can be seen for the viscosity of the nanofluid based on its volume fraction. Clearly, all the nanofluids follow a similar trend in temperature to that of the base fluid. However, as the volume fraction increases, there is an increase in the ratio of the nanofluid and the base fluid viscosity. This ratio also seems to diminish with an increase in temperature. This is the same general behaviour found by various research groups in the review done by Meyer et al. [3].

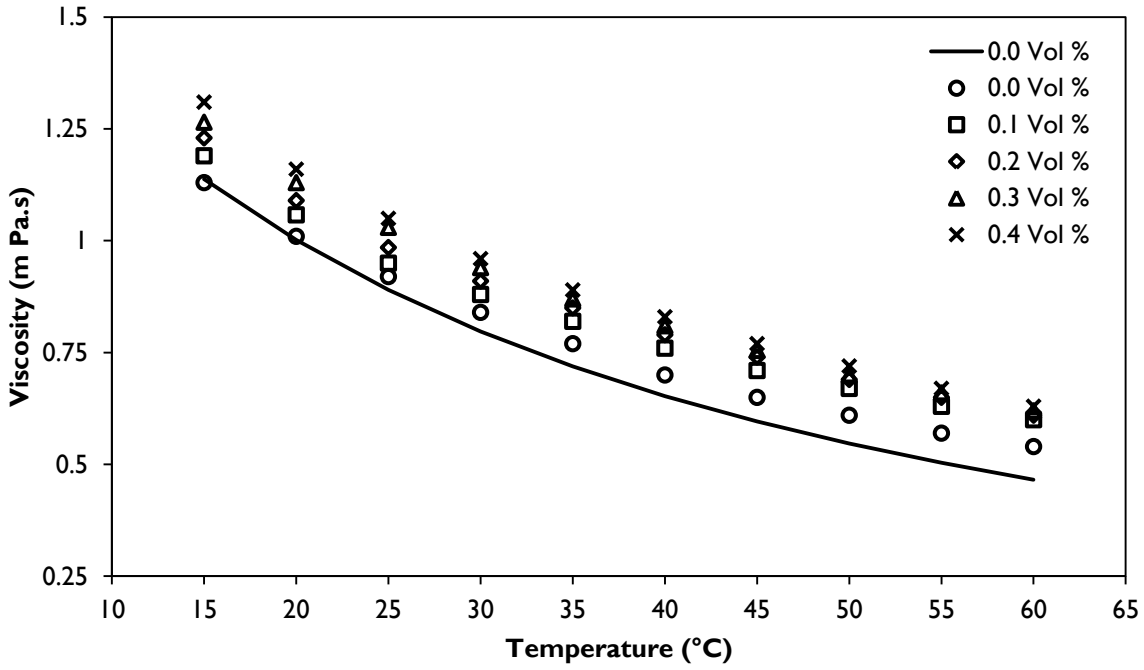

Figure 4: Viscosity of Fe_2O_3-H_2O as a function of temperature for various volume fractions

Using multivariate non-linear least-squares regression, the viscosity is fitted to a function:

$$\mu_{nf} = \mu_{bf}\left(1 + a\phi + b\phi\left(\frac{T}{T_0}\right)\right)^c \tag{3.1}$$

where $T_0 = 298.15K$.

The coefficients were found to be:

$$a = -3026.62$$
$$b = 3832.41$$
$$c = 0.0976826$$

The base fluid viscosity used in Equation 3.1 is obtained via a least-squares regression analysis of the experimentally acquired data, given as:

$$\mu_{bf} = 17.509\left(\frac{T}{T_0}\right)^2 - 40.31\left(\frac{T}{T_0}\right) + 23.725\ \text{mPa}\cdot\text{s} \tag{3.2}$$

The maximum error was found to be 3.05% with an average error of 1.22% and a coefficient of determination of $R^2 = 0.9959$.

Aybar et al. [1] and Sharifpur et al. [25] found that the error for thermal conductivity models is in the range of 5% for volume concentration below 1%. This error is comparable to that of the thermal conductivity meters available and so explicit measurement of the thermal conductivity has been omitted. The reasoning used here has also been applied by Ghodsinezhad et al. [20] in a similar study, but for Al_2O_3-water nanofluids. A study conducted by Karimi et al. [21] experimentally investigated the thermal conductivity of water-based Fe_2O_3 and Fe_3O_4 nanofluids for volume concentrations ranging from 0% to 4.8% and a temperature range of 20 °C to 60 °C. Empirical correlations were drawn for both nanofluids as a function of the volume fraction and temperature. The results of the curve fit for the Fe_2O_3 nanofluid are given as:

$$k_{nf} = k_{bf}\left(1 + \phi + 138.78\phi\left(\frac{T}{T_{min}}\right)\right)^{0.06754} \tag{3.3}$$

where k_b is the thermal conductivity of the base fluid and T_{min} is given as 20 °C. The maximum error of this correlation was found to be 3.48%, while the average error was found to be 0.65%

As obtained from the study conducted by Ramires et al. [28], the thermal conductivity is determined from the following set of equations:

$$k^* = -1.48445 + 4.12292(T^*) - 1.63866(T^*)^2 \tag{3.4}$$
$$k^* = \frac{k_{bf}}{k_{bf}(298.15)} \tag{3.5}$$

where k^* is the non-dimensionalised thermal conductivity and $T^* = T/298.15$ is the non-dimensionalised temperature. The study also determined that $k_{bf}(298.15) = 0.6065\ \text{W/mK}$. This correlation holds in the range from 274 K to 370 K.

To ensure the generality of Equation 3.3, the results are compared to a study conducted by Patel et al. [29], where a model that improves upon the model of Hemanth et al. (in Patel et al. [29]) is proposed by introducing the effects of micro-convection present in the nanofluid to the original model. The model was found to give an accurate prediction for a range of particle sizes between 10 nm and 100 nm, as well as a volume fraction between 1% and 8%. It also showed good correlation for different nanofluids with various particle materials, as well as base fluids. It was shown to be accurate between temperatures of 20 °C and 50 °C. This model is given as:

$$k_{eff} = k_{bf} + k_p\left(1 + c\frac{u_p d_p}{\alpha_b}\right)\left(\frac{d_b}{d_p}\right)\left(\frac{\phi}{1-\phi}\right) \tag{3.6}$$

where k_b and k_p are the thermal conductivity of the base fluid and the particle respectively, α_b is the thermal diffusivity of the base fluid, d_p is the particle diameter, d_b is the molecular size of the liquid, c is a constant that needs to be determined experimentally (however, it has been found that the model still makes an accurate prediction for most cases when a fixed value of 25 000 is used) and u_p is the Brownian motion velocity given as:

$$u_p = \frac{2k_B T}{\pi \mu d_p^2} \tag{3.7}$$

where k_B is the Boltzmann constant, T is the temperature and μ is the dynamic viscosity of the base fluid.

The results of both models can be seen in Figure 5 and Figure 6.

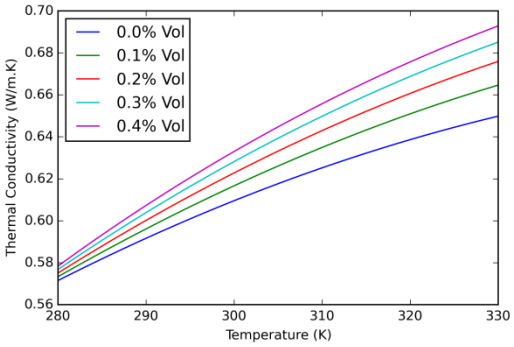

Figure 5: Thermal conductivity model of Karimi et al.[21]

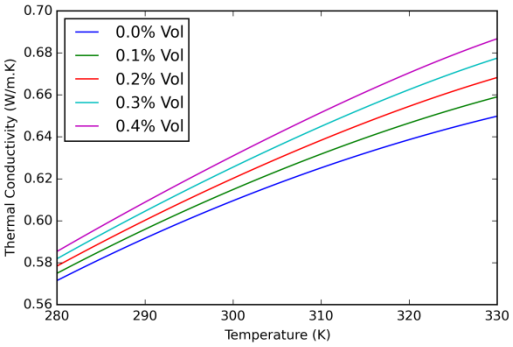

Figure 6: Thermal conductivity model of Patel et al. [29]

When considering the results of both models, a similar trend is observed. For the range between $290\ \mathrm{K}$ and $310\ \mathrm{K}$, very similar results are found. The model of Karimi et al. [21] predicts lower thermal conductivities at lower temperatures, while after approximately $290\ \mathrm{K}$, the models starts to predict a higher thermal conductivity when compared to the model of Patel et al. [27]. Overall, the models are in fair agreement with each other. Considering that the model proposed by Karimi et al. [21] is specifically fitted to the experimental data of an $Fe_2O_3 - H_2O$ nanofluid, while the model proposed by Patel et al. [27] is fitted to a wider variety of nanofluids, it was decided to use the former equation to predict the thermal conductivity of the nanofluids used in this study.

3.2 Stability

For the natural convection tests, it was desired to use a volume fraction in the range of 0.05% to 0.3%. However, it was found that nanofluids that are simply mixed with no additional steps taken to ensure stability are highly unstable considering that the rapid settlement of particles was observed visually in a matter of minutes for the poorest cases.

Two methods were investigated to improve the stability of the nanofluids. For lower volume fractions, the pH of the nanofluid was adjusted. For nanofluids with a volume concentration between 0.05% and 0.4%, the use of SDS as a stabiliser was investigated.

3.2.1 pH adjustment

When adjusting the pH of nanofluids of a higher volume concentration, this was found to have very little effect on the nanofluids' stability. As a way to work towards a stable nanofluid of a higher volume concentration, a study was conducted on the effects of pH adjustment for lower volume concentrations. For this study, nanofluids of $\phi = 0.001\%$ and $\phi = 0.005\%$ with the pH adjusted to 9.5 were prepared as discussed in section 2.1. The stability was analysed using a UV-visible spectroscopy reading obtained with a Jenway-7315 spectrophotometer. This was accompanied by visual stability analysis.

The visual stability results $\phi = 0.001\%$ and $\phi = 0.005\%$ can be seen in Figure 7 and Figure 8 respectively. Clear settlement can already be seen after the first day for both nanofluids. This being said, it seems as if the $\phi = 0.001\%$ shows much more rapid settlement, as a clear discolouration of the nanofluid can be seen throughout the upper section of the fluid. When looking at the $\phi = 0.005\%$, some settlement can be seen after the first hour. However, it seems that after initial settlement takes place, the settling process slows down when comparing the results at the 18-hour and 24-hour marks.

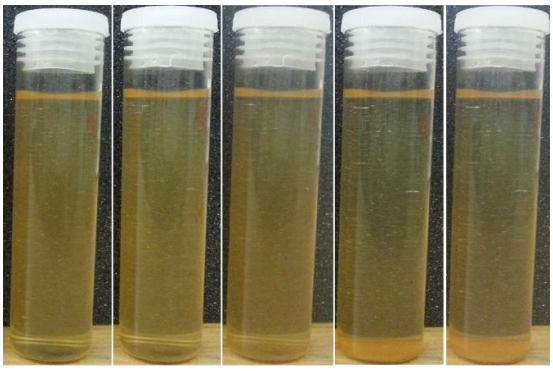

Figure 7: Nanofluid sample for $\phi = 0.001\%$ at: (a) t = 0 hours; (b) t = 1 hour; (c) t = 4 hours; (d) t = 18 hours; and (e) t = 24 hours

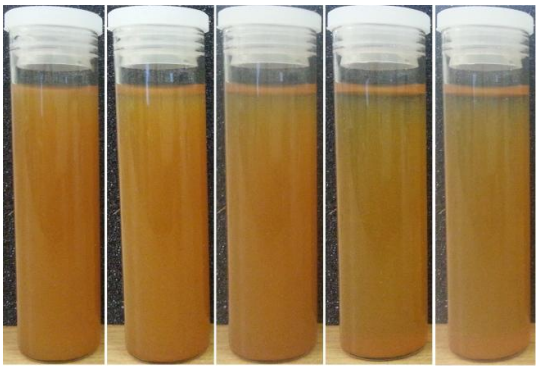

Figure 8: Nanofluid sample for $\phi = 0.005\%$ at: (a) t = 0 hours; (b) t = 1 hour; (c) t = 4 hours; (d) t = 18 hours; and (e) t = 24 hours

In order to analyse the stability of the nanofluid using UV-visible spectroscopy results, a full-spectrum scan was performed between $230\ \text{nm}$ and $900\ \text{nm}$ in increments of $1\ \text{nm}$ of the absorbance of both nanofluids directly after preparation was done. The point with maximum absorbance was found, which was given as $\lambda = 303\ \text{nm}$ for the $\phi = 0.001\%$ case and $\lambda = 298\ \text{nm}$ for the $\phi = 0.005\%$ case.

The absorbance of the nanofluid is then measured every 1 000 seconds at the wave length found to have the maximum absorbance. Figure 9 and Figure 10 show the results obtained from this method. The graphs more clearly demonstrate the same results as found in the stability analysis. When considering the response of the $\phi = 0.001\%$ case, a much lower stability is found compared to the $\phi = 0.005\%$ case. It can be seen that the $\phi = 0.001\%$ nanofluid almost immediately shows signs of instability with a negative slope at $t = 0\ \text{hours}$. However, it can be said that the nanofluid is stable

for at least two hours after preparation, after which settlement rapidly accelerates up to a certain point, seen here to be approximately $t = 12$ hours, after which the fluid reaches a new stable level. This explains why Figure 7 (a) and (b), as well as (d) and (e), are seen to be very similar, while (c) shows rather subtle signs of settlement.

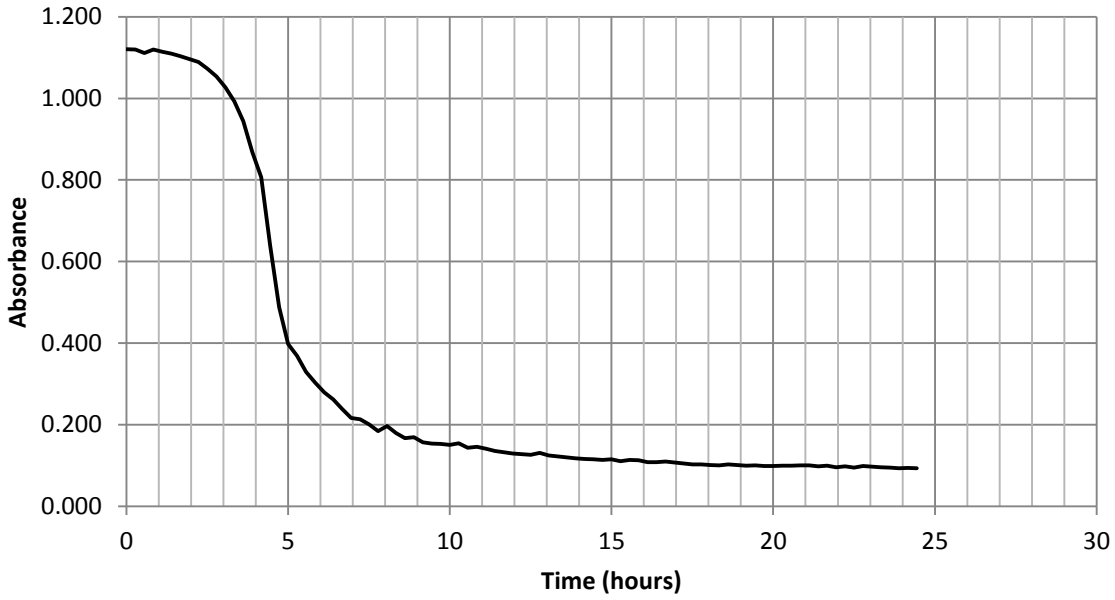

Figure 9: Time dependence of fluid absorbance over time for the $\phi = 0.001\%$ nanofluid

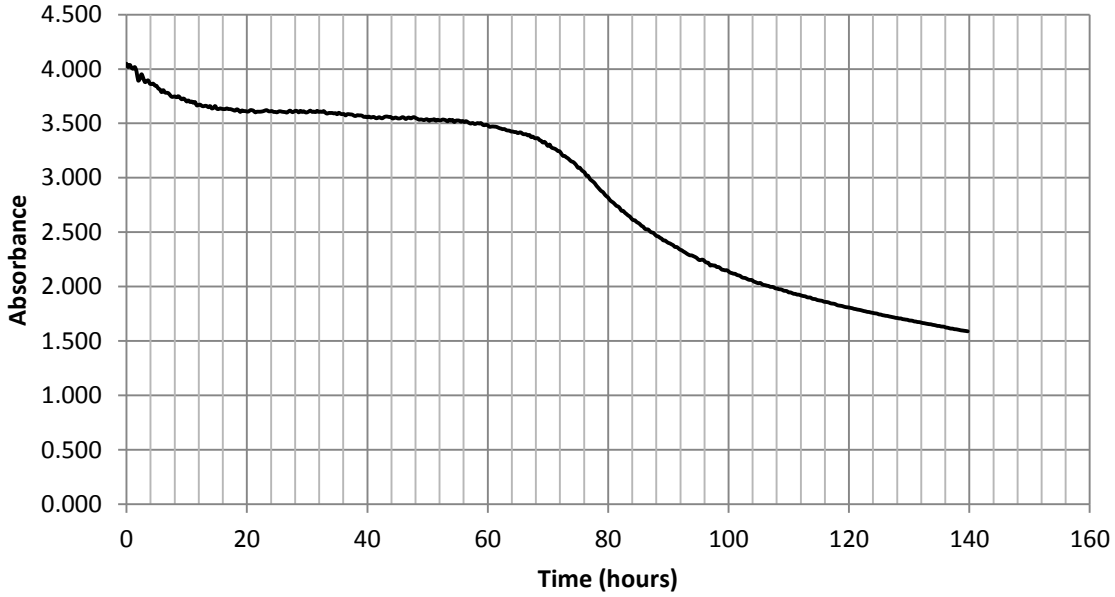

Figure 10: Time dependence of fluid absorbance over time for the $\phi = 0.005\%$ nanofluid

Considering the results of Figure 10, it is clear that a very different behaviour is found for the $\phi = 0.005\%$ nanofluid. Here it can be seen that a rather slow initial decay in absorbance is present over the first 20 hours or so, corresponding to the settlement of nanoparticles, after which a new stable level is reached. It can be seen that, in the region from $t = 20$ hours to $t = 60$ hours, slight

settlement is still present. However, for the most part, the nanofluid remains fairly stable. For the final section after $t = 60$ hours, rapid settlement is seen to take place.

As with the $\phi = 0.001\%$ case, this illuminates the reason why Figure 8 seems to show a slow decrease in particle concentration when scanning from (a) to (e).

A possible explanation for this is that, due to initial particle settlement, charged nanoparticle deposits form at the bottom of the container. These charged particles repel particles that are still dispersed in the nanofluid. This also explains why the lower volume fraction case did not perform as well, as it takes a much higher fraction of the total available particles to create a sufficient layer of settled particles.

When the pH was adjusted for nanofluids of a higher concentration, the results showed very poor performance. As mentioned in the literature, it is likely that these nanofluids require a stabiliser to receive the maximum benefit from pH adjustment.

One downfall of adjusting the pH of a nanofluid for stability reasons revolves around the fact that, if the pH is either too high or too low, the nanofluid may start to damage the equipment in which it is to be used.

3.2.2 Stabiliser

An initial stability analysis was carried out via visual inspection. To further determine the stability of the 0.4% as well as the 0.05% volume fraction, an additional stability analysis was carried out by measuring the viscosity of the nanofluid over a period of 20 hours at a fixed temperature. This gives a measure of stability since any change in viscosity (given that all operating conditions remain fixed) would be attributed directly to the settlement of the nanoparticles alone.

Figure 11 shows the pictures taken of the nanofluid with a 0.1% volume fraction over a period of 15 days. Similarly, Figure 12 shows the pictures taken of a nanofluid with a 0.4% volume fraction over the same period.

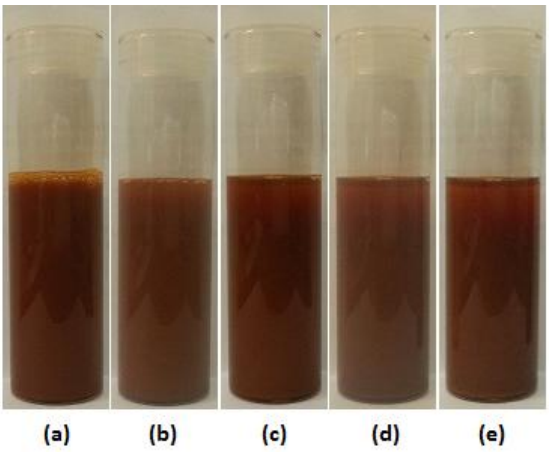

Figure 11: Nanofluid sample for $\phi = 0.1\%$ at: (a) t = 0 hours; (b) t = 24 hours; (c) t = 120 hours; (d) t = 240 hours; and (e) t = 360 hours

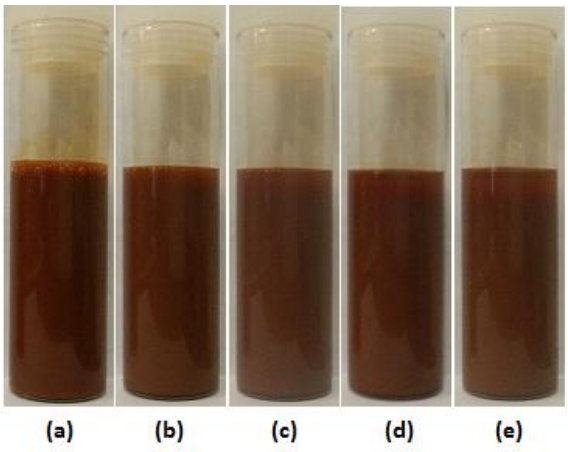

Figure 12: Nanofluid sample for $\phi = 0.4\%$ at: (a) t = 0 hours; (b) t = 24 hours; (c) t = 120 hours; (d) t = 240 hours; and (e) t = 360 hours

From visual inspection, it can be noticed that a nanofluid of a higher volume fraction has better stability when comparing the 0.4% case to the 0.1% case. Clear settlement was noticed on the fifth day for the 0.1% case, while the 0.4% case displayed a similar behaviour only after the tenth day.

Figure 13 and Figure 14 show the measured viscosity of the $\phi = 0.05\%$ and $\phi = 0.4\%$ cases respectively over a period of 20 hours. Measurements were taken every two minutes for the duration of the test.

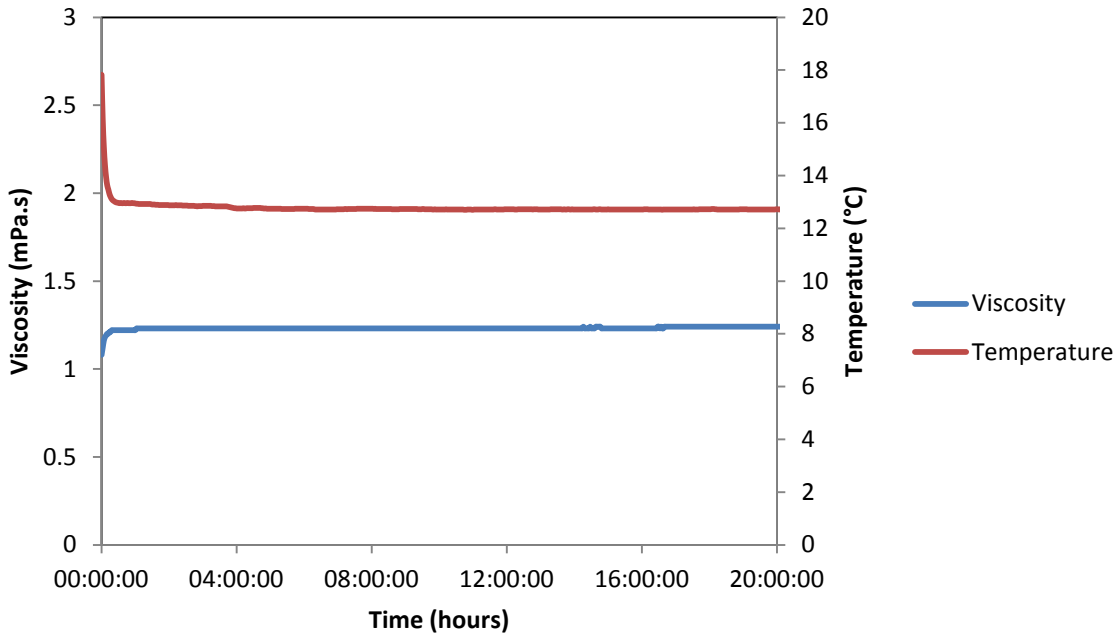

Figure 13: Viscosity vs. time for stability analysis for $\phi = 0.05\%$

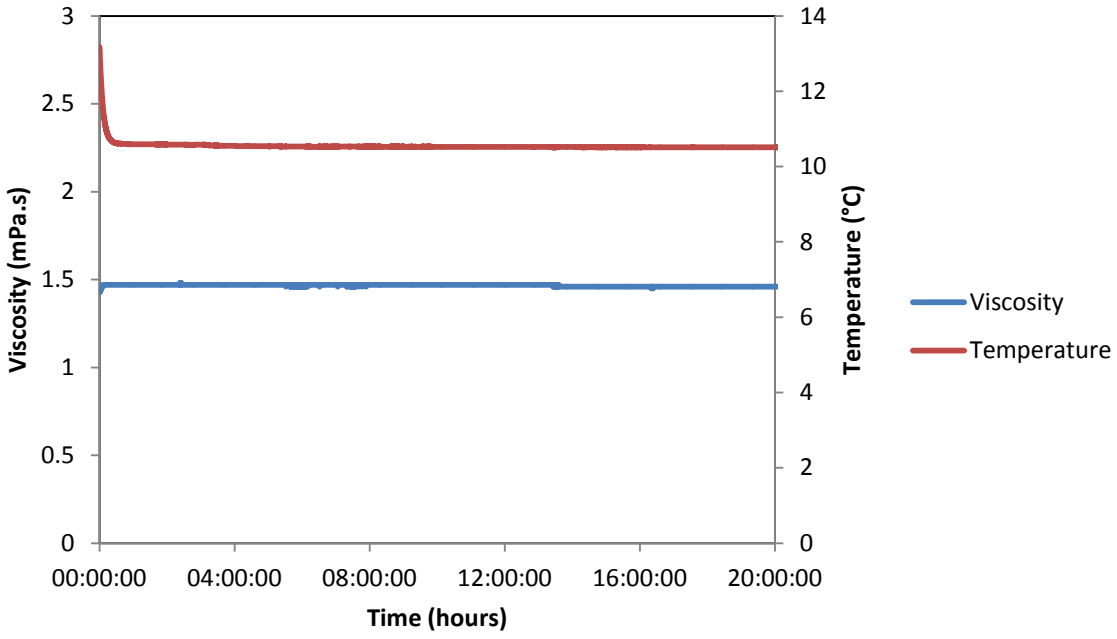

Figure 14: Viscosity vs. time for stability analysis for $\phi = 0.4\%$

Small fluctuations in the viscosity measurements can be seen under close inspection. The change in viscosity readings are most likely due to small vibrations caused by other lab equipment rather than the settlement of the nanoparticles, as these changes are not only very small, but seem to fluctuate randomly as well.

The visual inspection shows that, even with the addition of a stabiliser, the nanoparticles are still settling, albeit at a much slower rate. However, the viscosity-based stability study shows that this is not a problem for the experiment, as each nanofluid is only be used over a period of at most six hours, which is clearly much lower than the settling time required to change the nanofluid properties by a measureable amount.

3.3 Nanoparticle sizes

A transmission electron microscopy (TEM) analysis was done to determine the approximate sizes of the nanoparticles. The results of the TEM analysis can be seen in Figure 15 and Figure 16.

On average, the size of the nanoparticles was found to fall within the range of 15 to 20 nm, showing a good correlation with the information provided by the manufacturer.

A zetasizer should be used to get a better estimate of the size of the nanoparticles present in the nanofluid. It would also enable one to determine the average particle size as a function of sonication time or, more specifically, sonication energy input.

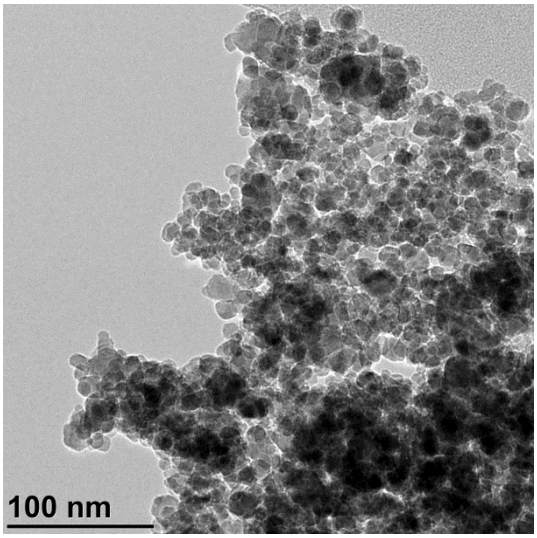

Figure 15: TEM analysis results – coarse scale

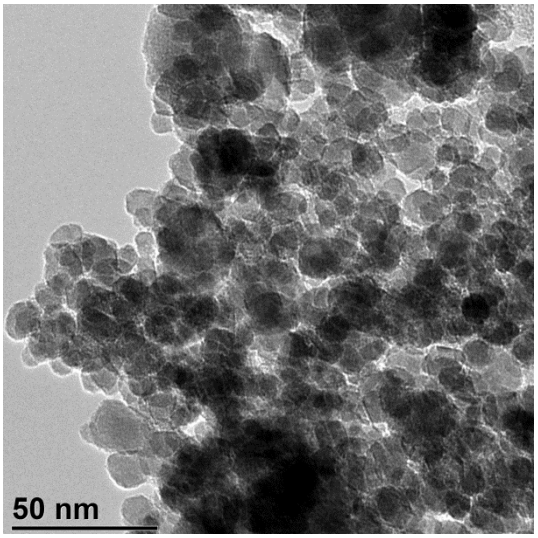

Figure 16: TEM analysis results – fine scale

3.4 Conclusion

When considering the viscosity obtained for all the tested nanofluids, it is clear that a similar trend is observed to those found in other studies, namely that the viscosity increases with an increase in volume concentration. It was also found that the viscosity does not increase by a constant factor for all temperatures, but rather that this factor is a function of temperature as well. A similar form to the chosen thermal conductivity model (as seen in Equation 3.3) fits the viscosity data well.

Since the thermal conductivity data could not be measured for the tested nanofluids, an empirical model for similar nanofluids is used. The thermal conductivity model that was chosen shows similar behaviour to a general model for various nanofluids. This inspires confidence in this model since it shows behaviour that is not only expected, but also repeatable by many different groups.

The stability results show unexpected behaviour. For both methods, it was seen that lower volume concentrations have poorer stability. This being said, all volume concentrations desired to be used in the cavity fall within the bracket where sufficient stability is shown. It was found that, while adjusting the pH had a fair effect on the stability of nanofluids of a low concentration, at a higher concentration, it has a minute effect. When considering the effects of SDS on the stability of the nanofluids, it is clear that this had a considerable effect, as nanofluids that would show rapid settlement visually after a matter of hours, remained visually stable for weeks. Considering the stability results for the viscosity-based tests for both $\phi = 0.05\%$ and $\phi = 0.4\%$, it is clear that the stability is acceptable for natural convection tests. However, the visual stability results show that a more stable nanofluid needs to be prepared for longer-running systems. The effects of using a stabiliser in conjunction with pH adjustments were not tested. However, based on the results from the literature, there is reason to believe that this would improve the stability of the nanofluid even further. The size of the nanoparticles was determined via TEM analysis. However, the agglomerate size as a function of mixing time or, more specifically, energy density, should be determined to obtain more information about particle sizes in the fluid and for more insight into the stability behaviour of the nanofluid.

Chapter 4: Results

The study focused on two main aspects to determine how iron oxide nanofluids can be used to increase heat transfer due to natural convection. The first was to consider only the effects of introducing nanoparticles into the base fluid as a pure nanofluid, while the second considered the effects of an externally applied magnetic field on the nanofluid.

The results of both studies are presented in a systematic fashion showing the analytical process that was followed.

The first set of results that is presented is the temperature of the fluid inside the cavity. This is followed by presenting the difference between the heat introduced into the system and the heat removed from the system. To start quantifying the performance of the nanofluids, heat transfer through the system was compared based on the wall temperature difference of the cavity for all cases of interest in the particular study. Using these results, the heat transfer coefficient was presented as a function of the wall temperature difference followed by the Nu as a function of the wall temperature difference for each case. Finally, a comparison was made between the Nu for a specific Ra.

4.1 Influence of nanoparticle concentration

As mentioned in section 2.2, the thermal baths on the hot side were tested at 40 °C, 45 °C, 50 °C and 55 °C, while the corresponding temperatures on the cold side were set to 20 °C, 15 °C, 10 °C and 5 °C. The results presented in Figure 17 to Figure 22 show the recorded temperature of the fluid inside the cavity along the mid-plane of the cavity.

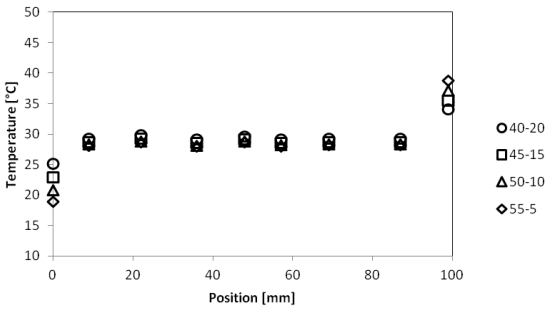

Figure 17: Fluid temperature for $\phi = 0.0\%$

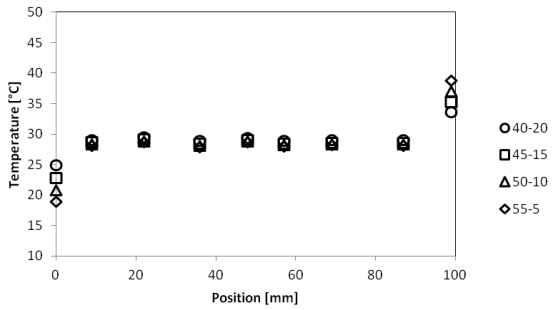

Figure 19: Fluid temperature for $\phi = 0.1\%$

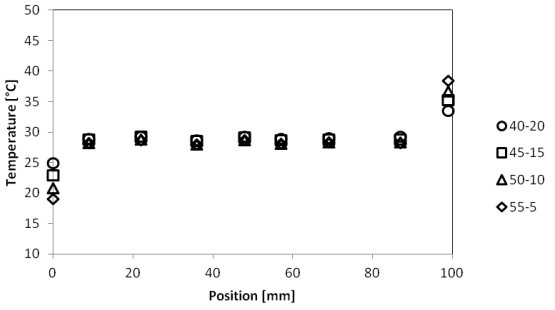

Figure 18: Fluid temperature for $\phi = 0.05\%$

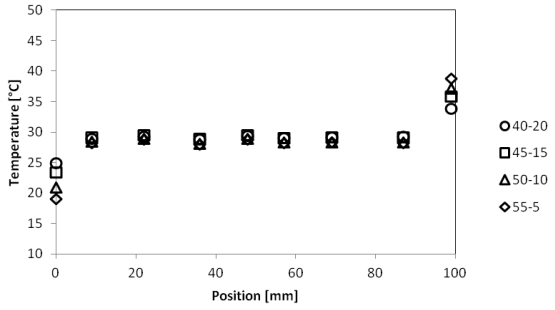

Figure 20: Fluid temperature for $\phi = 0.15\%$

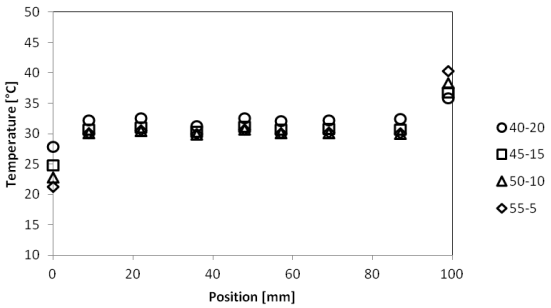

Figure 21: Fluid temperature for $\phi = 0.2\%$

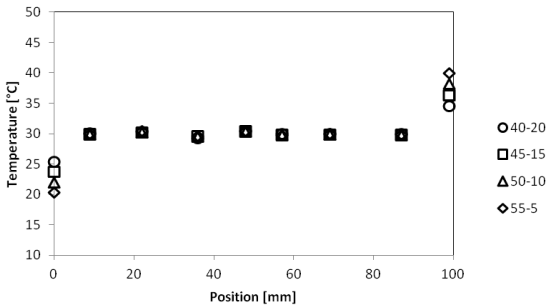

Figure 22: Fluid temperature for $\phi = 0.3\%$

Each figure shows the fluid temperature for all four thermal bath configurations (presented as hot-cold thermal bath temperature in the legend) used for a specific fluid based on its volume concentration. The reading at x = 0 mm gives the cold wall temperature while the reading at x = 99 mm gives the hot wall temperature at the centre of the wall for each thermal bath configuration.

The next set of results is used to determine how much of the heat that leaves the heat exchanger from the hot side is fully transferred through the system. The main goal of adjusting the flow rate from the thermal baths is to minimise this difference. This is due to the fact that a cavity with differentially heated walls in a steady state will transfer all the heat received at the hot wall to the cold wall. Adjusting the flow rate limits the available heat to allow the nanofluid to effectively transfer most of the heat through the system, minimising other losses, and ensuring that the system studied is a good approximation of the desired problem.

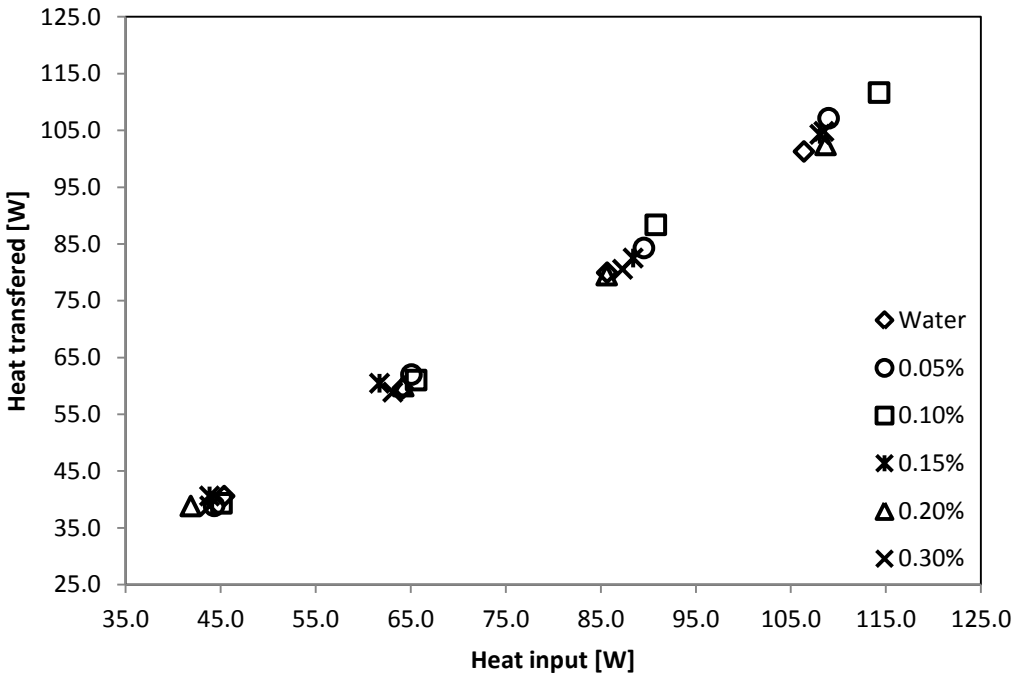

Figure 23: Relationship between supplied heat and heat transferred through the system

When considering the trend observed in Figure 23, one can see that not only does a linear trend present itself, but there is also approximately a one-to-one ratio between the heat input and the heat transferred out of the system.

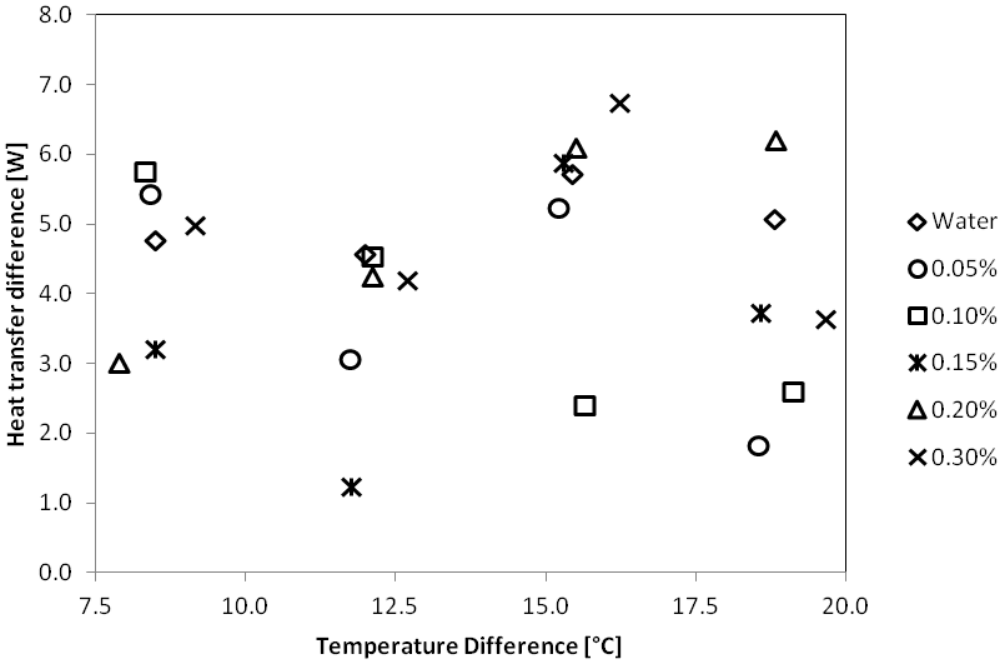

Figure 24: Difference in heat transfer as opposed to the wall temperature difference

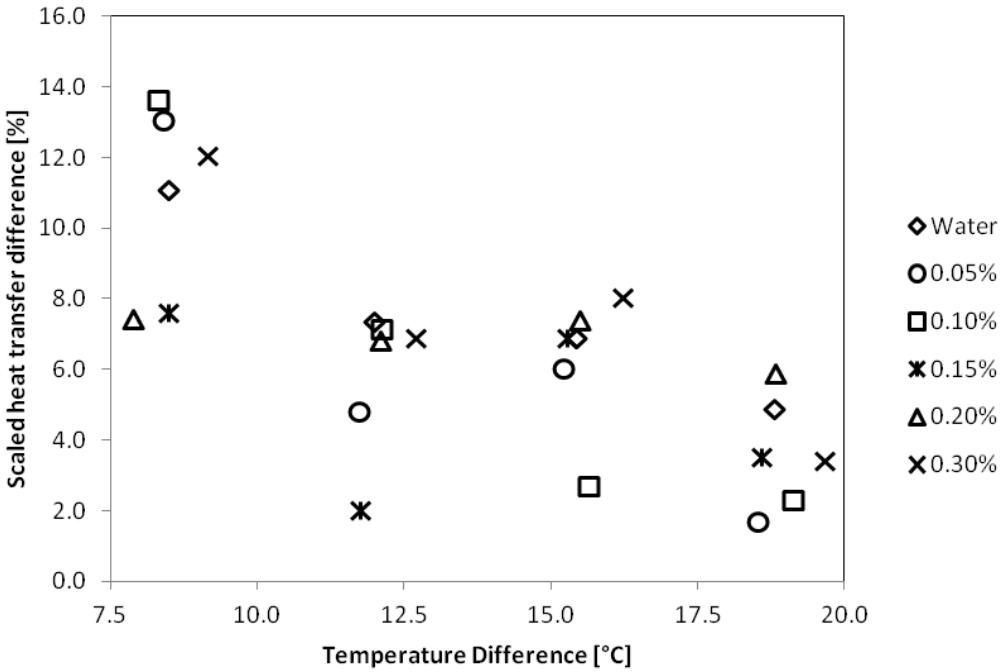

Figure 25: Scaled difference in heat transfer as opposed to the wall temperature difference

Figure 24 is used to present the difference between heat input and transferred heat based on the wall temperature difference, while Figure 25 presents the scaled heat transfer difference, defined as

$(Q_h - Q_c)/Q_{avg}$, as a function of the wall temperature difference. From these results, it can be seen that most of the heat leaks in the system are in the same range, from 2.5 W to 6.0 W, regardless of operating condition. It can also be seen that the scaled heat transfer difference is higher for lower wall temperature differences. This is expected since the heat transfer is driven by the wall temperature difference, and so the effects of heat leaks are more significant at lower wall temperature differences. The scaled heat transfer difference has a maximum value of 13.66% and an average value of 6.72%.

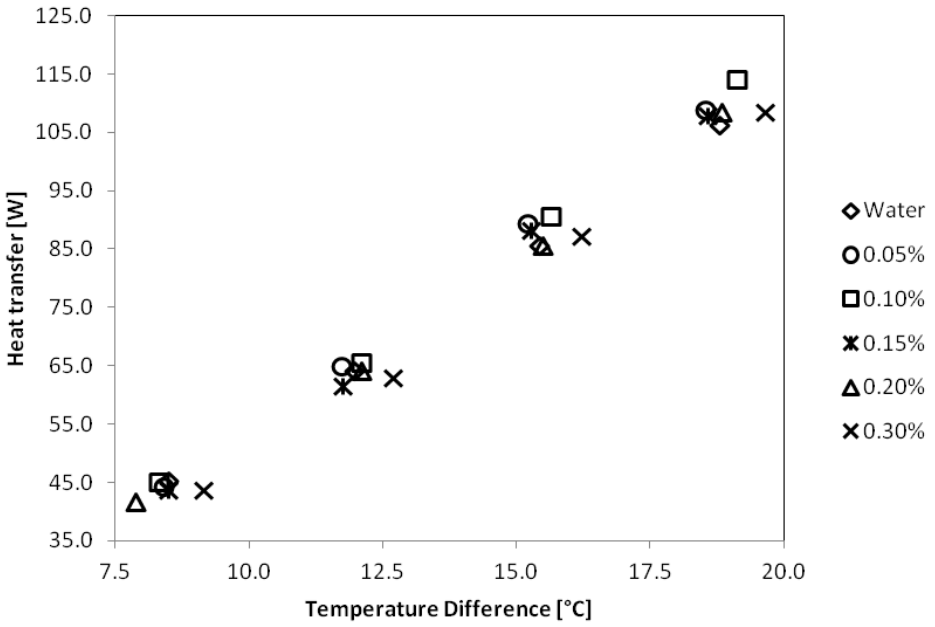

Figure 26: Heat transfer at the hot wall as a function of the wall temperature difference

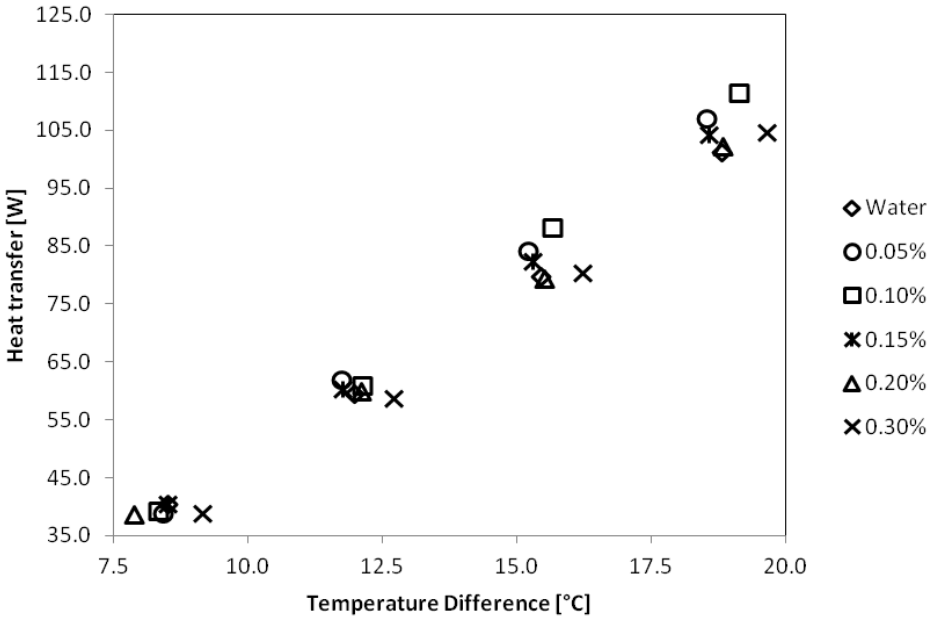

Figure 27: Heat transfer at the cold wall as a function of the wall temperature difference

The next set of results shows the relationship between the heat transfer and the wall temperature difference for the tested fluids. The heat transfer at the hot wall can be seen in Figure 26, while the heat transfer at the cold wall can be seen in Figure 27. Furthermore, the heat transfer at each side is used to determine the average heat transfer coefficient for the hot and the cold side. These results are presented in Figure 28 and Figure 29 respectively.

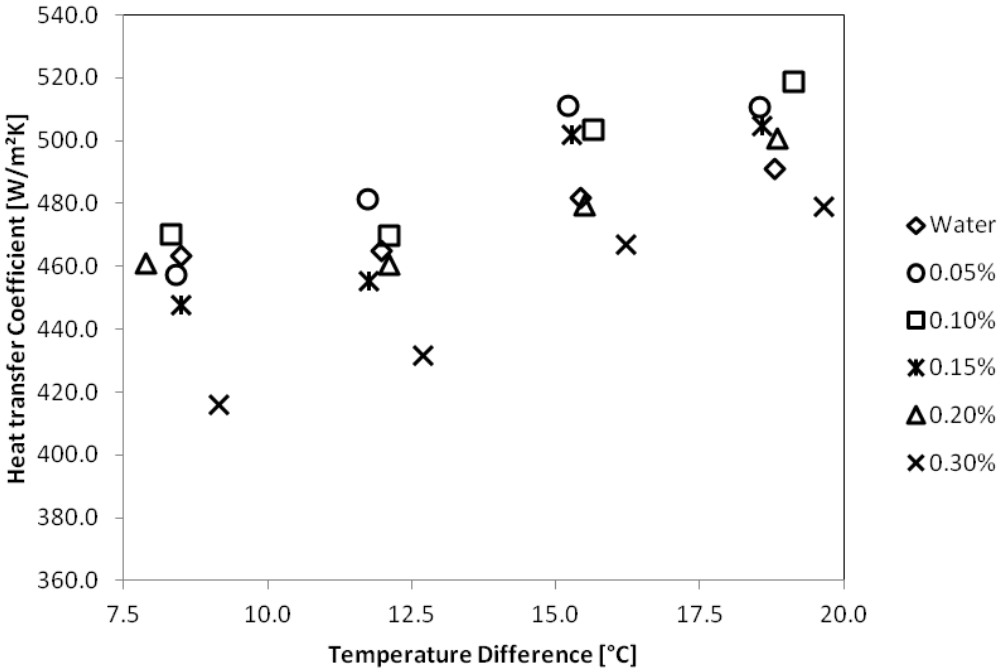

Figure 28: Heat transfer coefficient at the hot wall as a function of the wall temperature difference

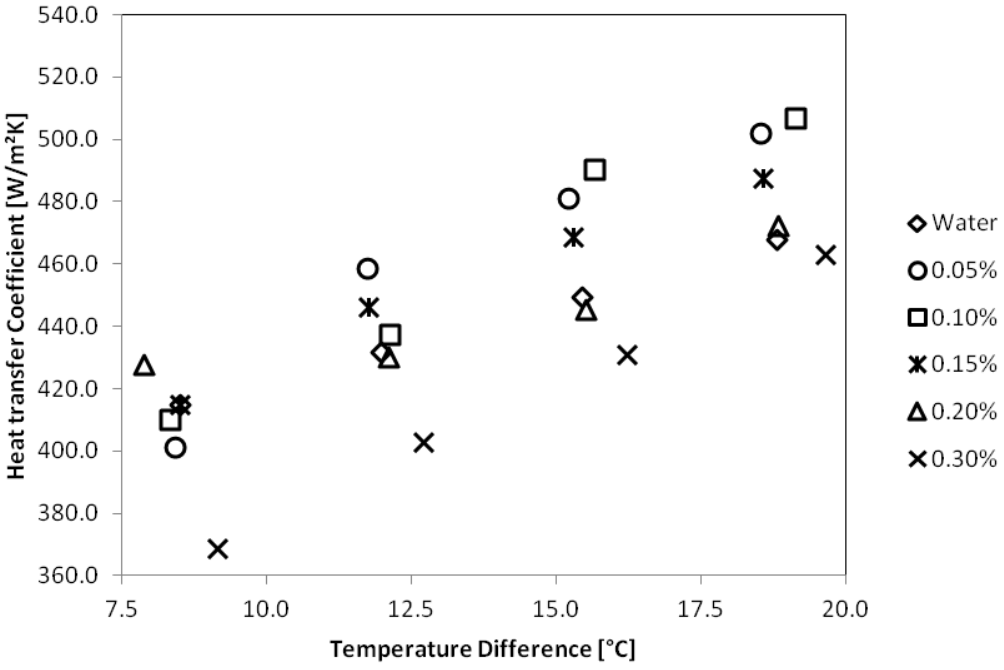

Figure 29: Heat transfer coefficient at the cold wall as a function of the wall temperature difference

One can see that there is not a large difference in heat transfer for the different volume fractions tested. However, the effects of the nanoparticles can be seen more clearly when one looks at the heat transfer coefficient.

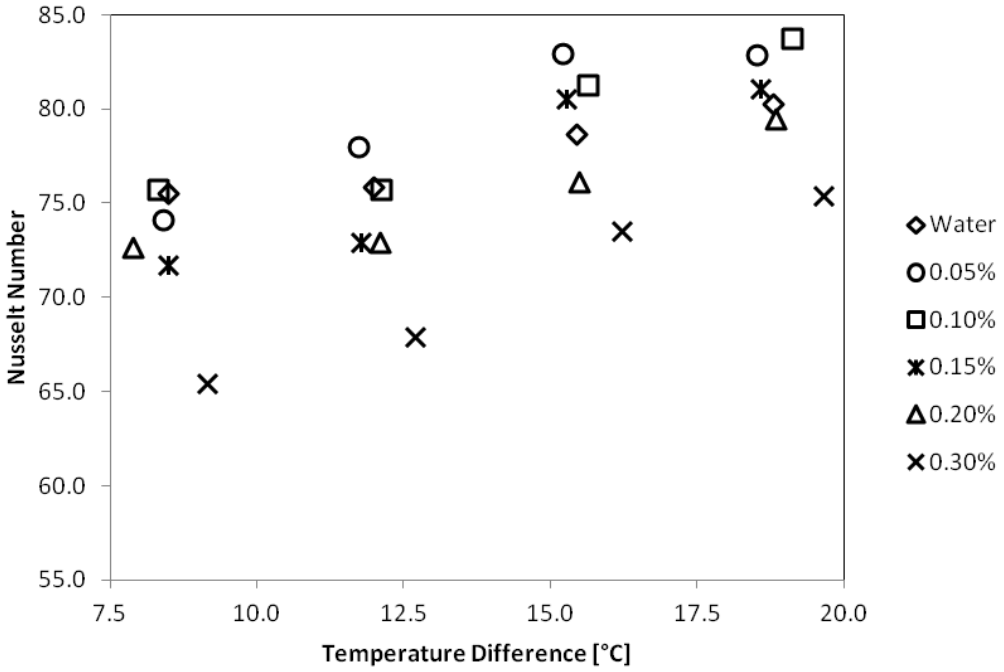

Figure 30: Nusselt number at the hot wall as a function of the wall temperature difference

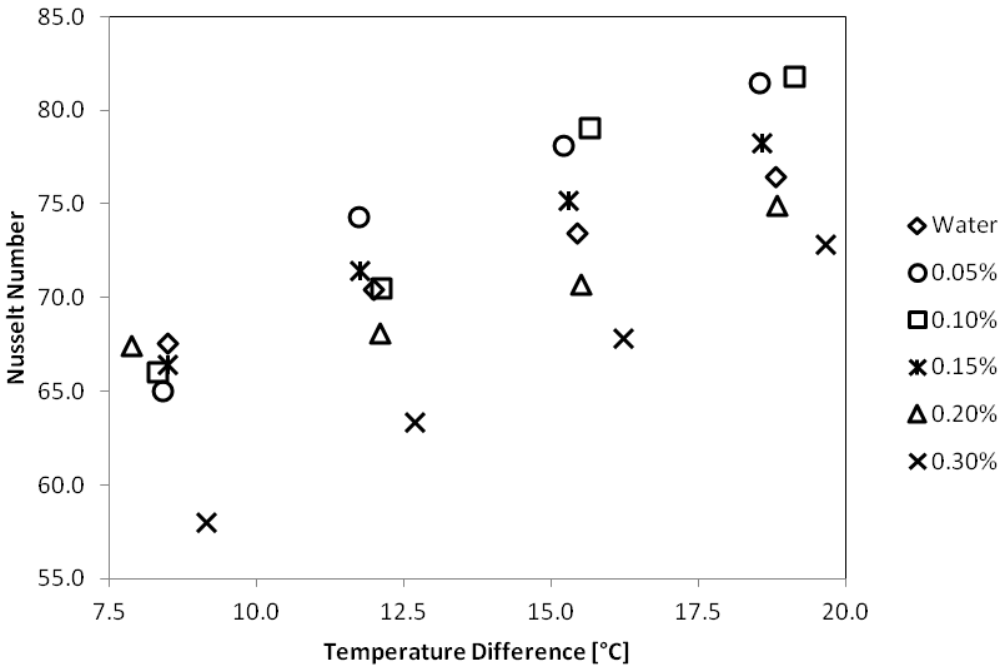

Figure 31: Nusselt number at the cold wall as a function of the wall temperature difference

When comparing the behaviour of the nanofluids to that of the base fluid case, one can see that, for all cases, there is clearly an optimum concentration that allows for maximum heat transfer. The

optimum concentration depends on the operating condition, but what is clear is that, after a certain concentration, the performance of the nanofluid deteriorates rapidly, as can be seen with the $\phi = 0.3\%$ case. When looking at these results, one can see that, for the majority of points for a volume fraction of 0.05%, 0.1% and 0.15%, the nanofluid has an enhanced performance compared to the base fluid, while the 0.2% case behaves in a similar fashion as the base fluid. Furthermore, the 0.05% and 0.1% volume fractions are seen to behave in a very similar manner to each other, with a high enhancement of heat transfer, making both very good candidates for the heat transfer fluid of this natural convection system. The maximum heat transfer coefficient for all cases was found to be the 0.1% volume concentration at a temperature difference of 19.1281°C with $h_c = 506.80\ \mathrm{W/m^2K}$ and $h_h = 518.64\ \mathrm{W/m^2K}$ for the cold and the hot wall respectively.

It should be noted that the behaviour at the lowest temperature difference does not follow a similar trend to the later points. It can be seen that the points are more closely grouped, with the exception of the 0.3% volume fraction case. This can be explained by the results presented earlier, dealing with the difference in the supplied and transferred heat, essentially introducing much higher uncertainty in the values at the lower temperature differences.

The Nu at the hot and the cold side is shown in Figure 30 and Figure 31 respectively. As expected, the same conclusions that are drawn for the heat transfer coefficient's behaviour are also applicable to the behaviour of the Nu.

The average Nu for the various nanofluids, which are simply the average between the hot- and the cold-wall Nusselt numbers, are compared at a similar Ra with the Ra for each nanofluid being determined by using its specific thermophysical properties obtained as described in chapter 2 and 3. These results are presented in Figure 32. From these results, it can be seen that both the 0.1% and the 0.05% volume concentrations behave much better than the other fluids. The 0.15% volume concentration also has an increased Nu when compared to the base fluid, but has a poorer performance compared to the nanofluids at both 0.05% and 0.1% volume concentrations. Due to the similar heat transfer behaviour, but increased thermal conductivity, the 0.2% volume concentration is actually seen to behave poorer than the base fluid, with the 0.3% volume concentration behaving the poorest out of all the tested fluids.

Finally, Figure 33 presents the average Nu over all the runs per volume fraction. The average is determined using a discrete integration scheme, specifically a trapezoidal integration method, given as:

$$\overline{Nu} = \left(\frac{1}{Ra_4 - Ra_1}\right)\sum_{i=1}^{3}\frac{1}{2}(Nu_i + Nu_{i+1})(Ra_{i+1} - Ra_i) \tag{4.1}$$

where Nu_i and Ra_i are the Nu and the Ra at the i^{th} measurement respectively.

Here it can clearly be seen that the 0.05% and 0.1% volume concentrations behave in a similar manner in terms of the increase in heat transfer performance, with $\phi = 0.05\%$ providing the best performance throughout the different operating conditions with an overall increase of 3.75%, with the $\phi = 0.1\%$ following closely behind with a 2.5% increase in the overall Nu. The 0.15% volume concentration behaves almost the same as the base fluid, with an increase of 0.03% in the overall

Nu. The 0.2% and 0.3% volume concentrations show negative results with a Nu deterioration of 3.00% and 8.91% of that of the base fluid respectively.

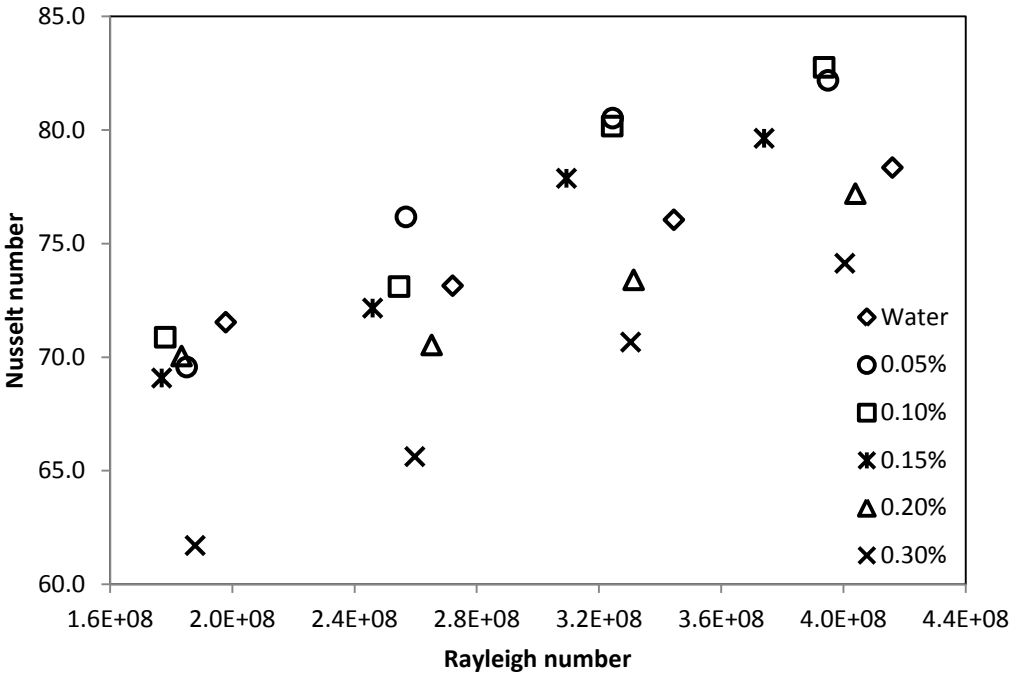

Figure 32: Nusselt number as a function of the Rayleigh number

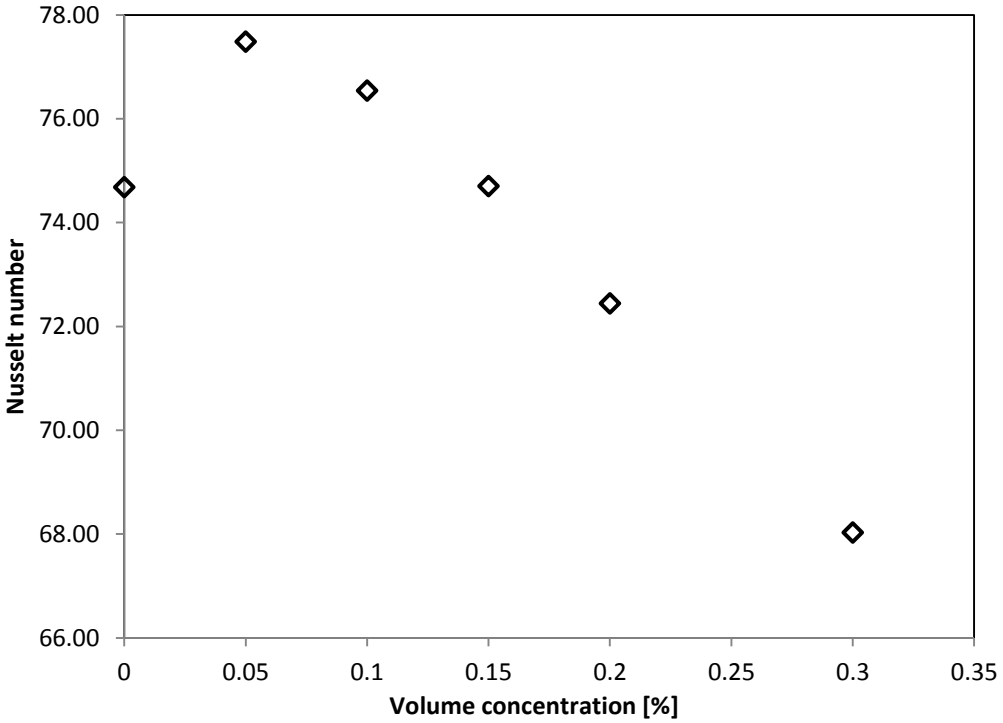

Figure 33: Average Nusselt number as a function of volume concentration

Both these and the previous results point to a possible maximum increase in heat transfer performance in the 0.05% to 0.1% volume concentration range, possibly with the exception of a maximum heat transfer performance at a volume concentration lower than 0.05% for a lower Ra.

4.2 Magnetic field influence

The effects of different magnetic fields on the heat transfer performance of a nanofluid are only determined for the 0.1% volume concentration case since this nanofluid showed a maximum increase to Nu at the maximum Ra. From the results given in section 4.1, there is reason to believe that if a 0.05% volume concentration nanofluid is used, the heat transfer performance would have an even greater response to the magnetic field, especially in the case where enhancement is indeed found. However, due to the results of section 3.2, where the stability is found to be poorer for fluids of a lower volume concentration, coupled with the possibility of higher settlement rates due to the additional magnetic force on the nanoparticles, the nanofluid of choice for this study was found to be a fluid with a 0.1% volume concentration.

In this section, the results are labelled using the letters (a), (b) and (c) to denote which configuration (as described in Figure 2) was used, as well as to specify the surface flux of the magnet used. The results of the base case are those for the 0.1% volume concentration with no magnetic field.

The fluid temperature for the six tested cases can be seen in Figure 34 to Figure 39.

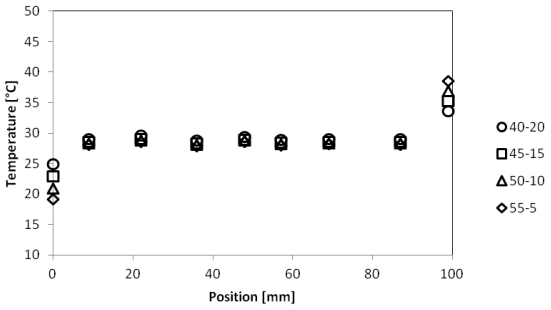

Figure 34: Fluid temperature for configuration 300 G (a)

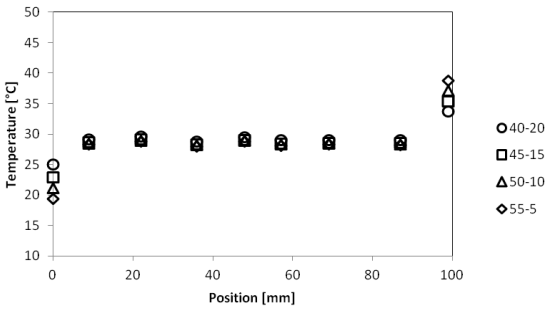

Figure 35: Fluid temperature for configuration 300 G (b)

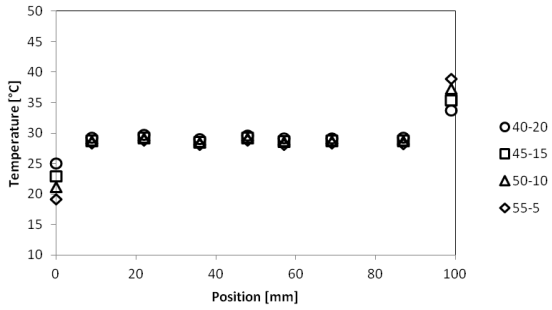

Figure 36: Fluid temperature for configuration 300 G (c)

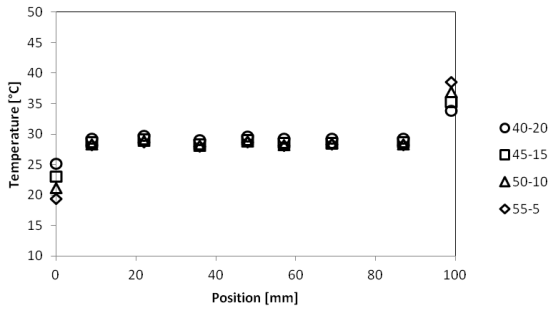

Figure 37: Fluid temperature for configuration 700 G (a)

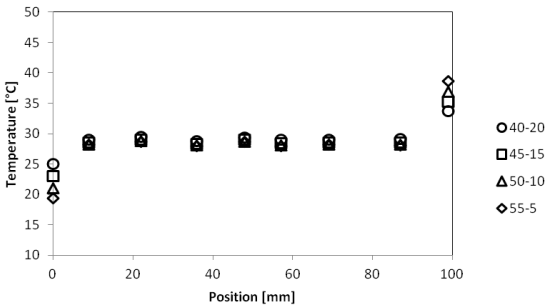

Figure 38: Fluid temperature for configuration 700 G (b)

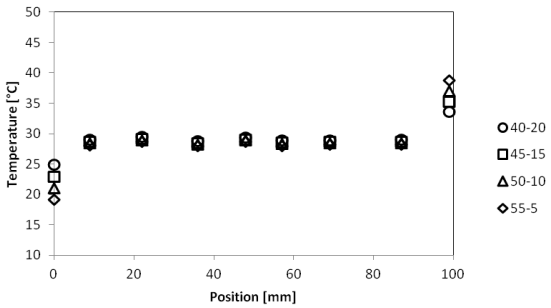

Figure 39: Fluid temperature for configuration 700 G (c)

The heat transferred to input heat ratio can be seen in Figure 40. As desired, there is a linear relationship between heat input and heat transferred with a gradient close to unity for each test.

A more detailed analysis of the difference between the heat transfer and input heat can be seen in Figure 41 and Figure 42. A similar result to the zero magnetic field case is found, specifically that the difference in heat transferred and heat input is, for the most part, in the same range, starting at approximately 2.5 W and ending at 6.0 W, regardless of operating condition. When looking at the scaled difference in heat transferred and heat input, the maximum errors are found at lower wall temperature differences.

Moving on to the heat transfer results, Figure 43 and Figure 44 show the heat transfer at the hot and the cold walls respectively, as a function of wall temperature differences, while Figure 45 and Figure 46 show the average heat transfer coefficients as a function of the wall temperature differences.

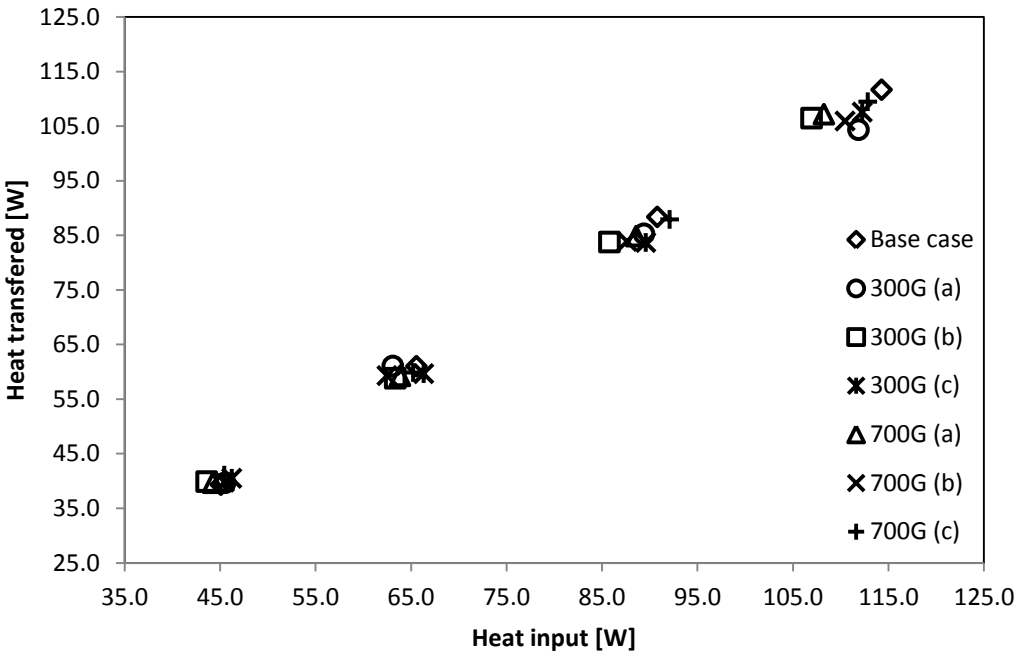

Figure 40: Relationship between the supplied heat and the heat transferred through the system

When one looks at the results of the heat transfer throughout the system, one can see that the heat transfers for all cases are close to each other. No single configuration can, therefore, be said to have any major impact on the heat transfer throughout the system. It can be seen that the 700 G (c) case

performs slightly better than the other cases, while the 300 G (b) case performs the poorest out of the tested cases.

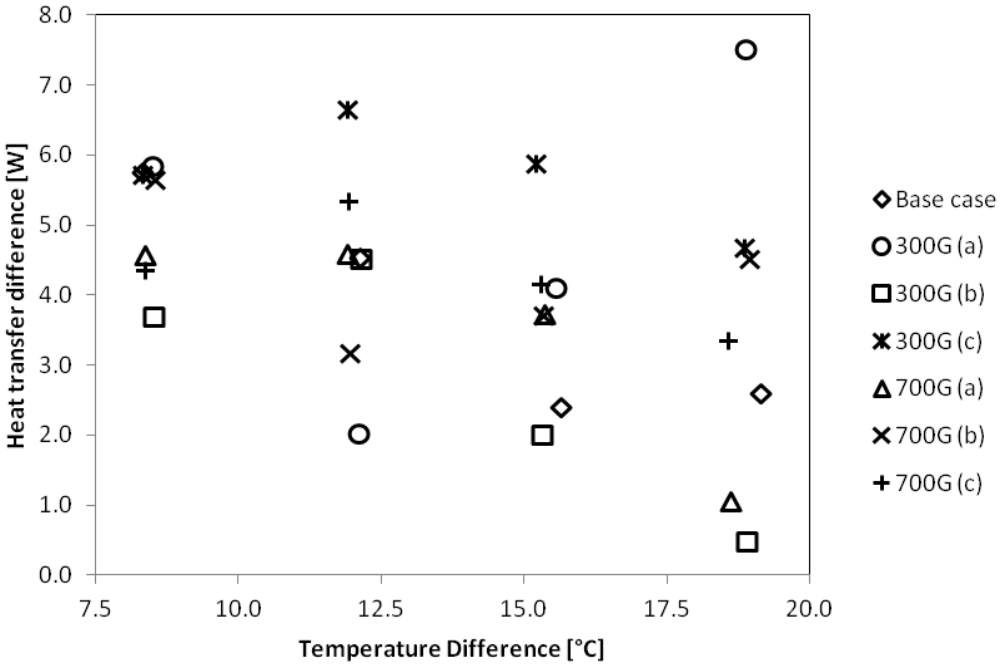

Figure 41: Difference in heat transfer as opposed to the wall temperature difference

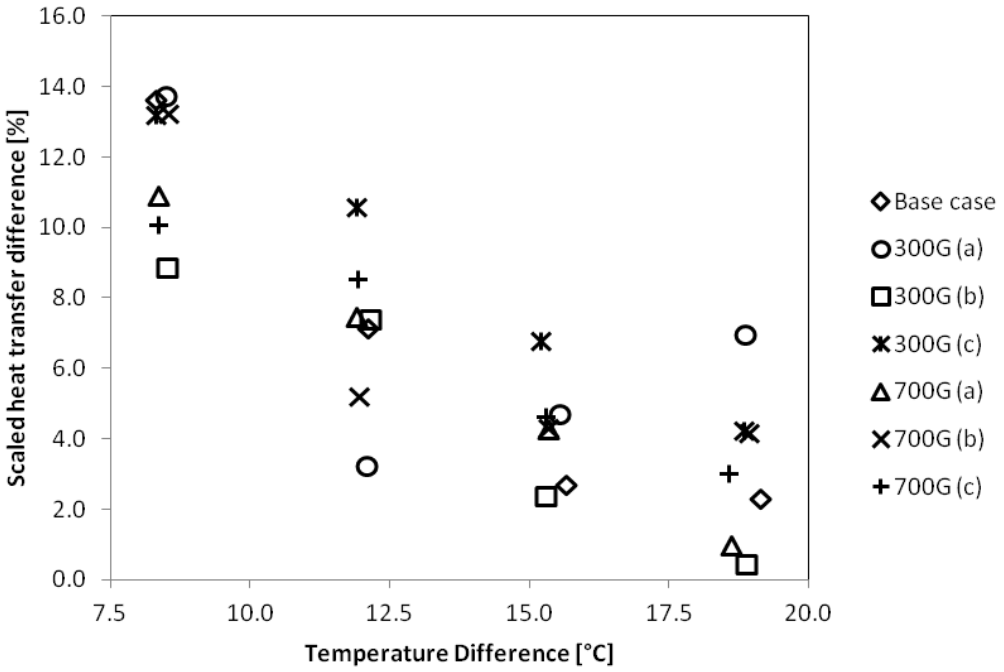

Figure 42: Scaled difference in heat transfer as opposed to the wall temperature difference

When one looks at the results for the heat transfer coefficient, the trends present in the heat transfer results become more illuminated. From these results, one can see that only two of the configurations perform better than the base case.

The first configuration to consider is the 300 G (c) case, where there is an increase in performance at lower temperature differences. However, as the temperature increases, the performance starts to fall behind the base case's performance. The 700 G (c) configuration is the only case that outperforms the base case at every point. The maximum heat transfer coefficient for this case was found to be at the temperature difference of $18.575\,℃$ with $h_h = 527.32\,\mathrm{W/m^2K}$ and $h_c = 511.62\,\mathrm{W/m^2K}$ for the hot and the cold walls respectively.

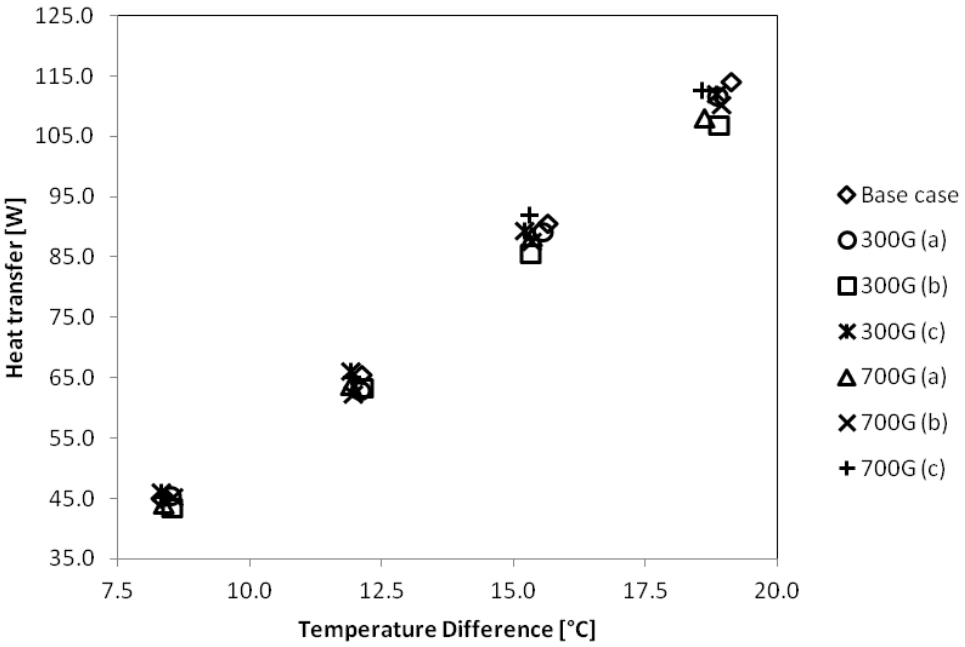

Figure 43: Heat transfer at the hot wall as a function of the wall temperature difference

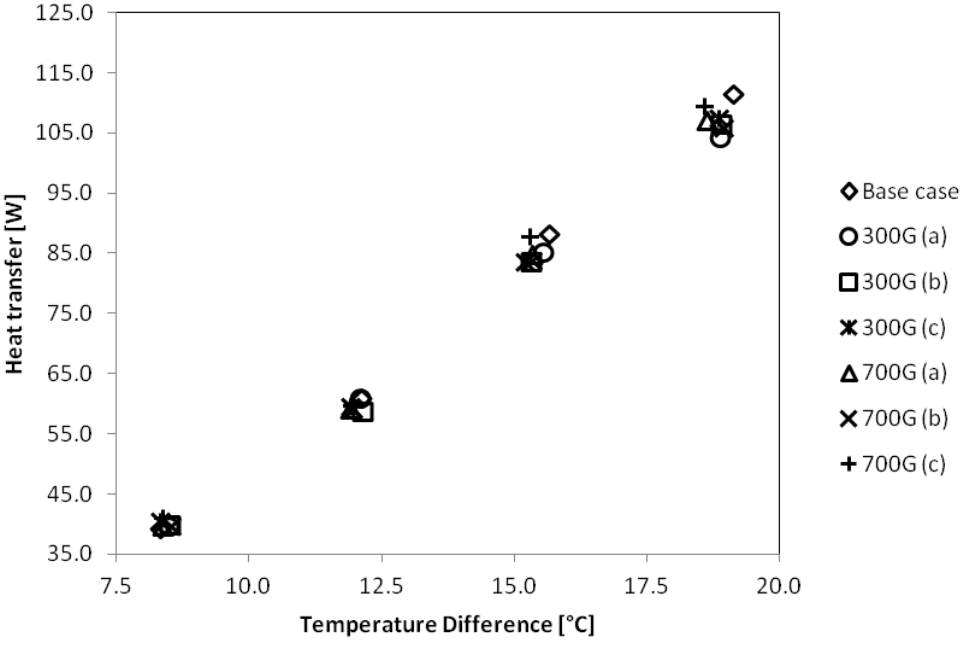

Figure 44: Heat transfer at the cold wall as a function of the wall temperature difference

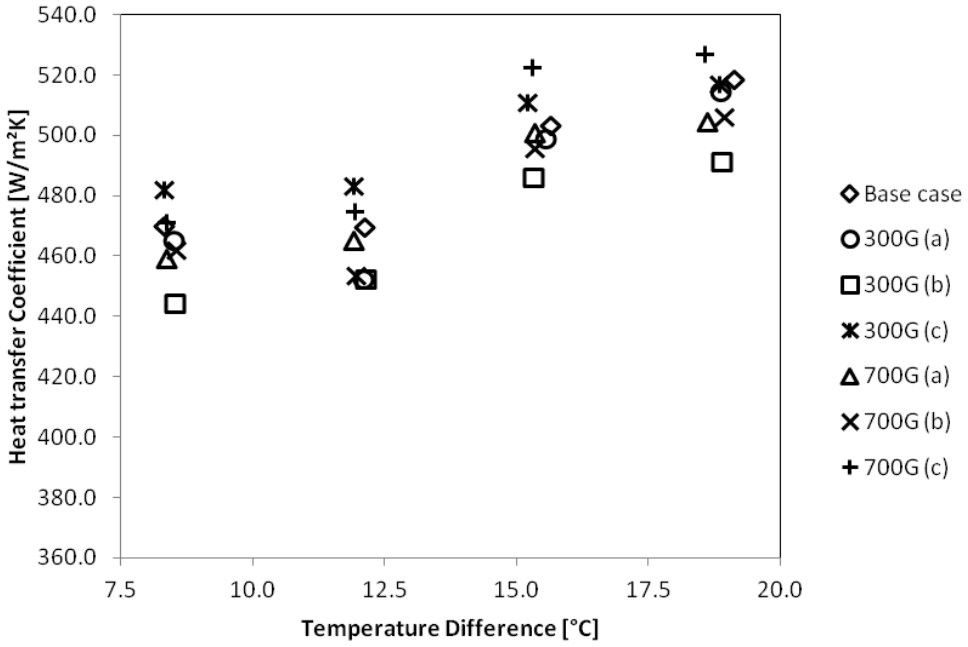

Figure 45: Heat transfer coefficient at the hot wall as a function of the wall temperature difference

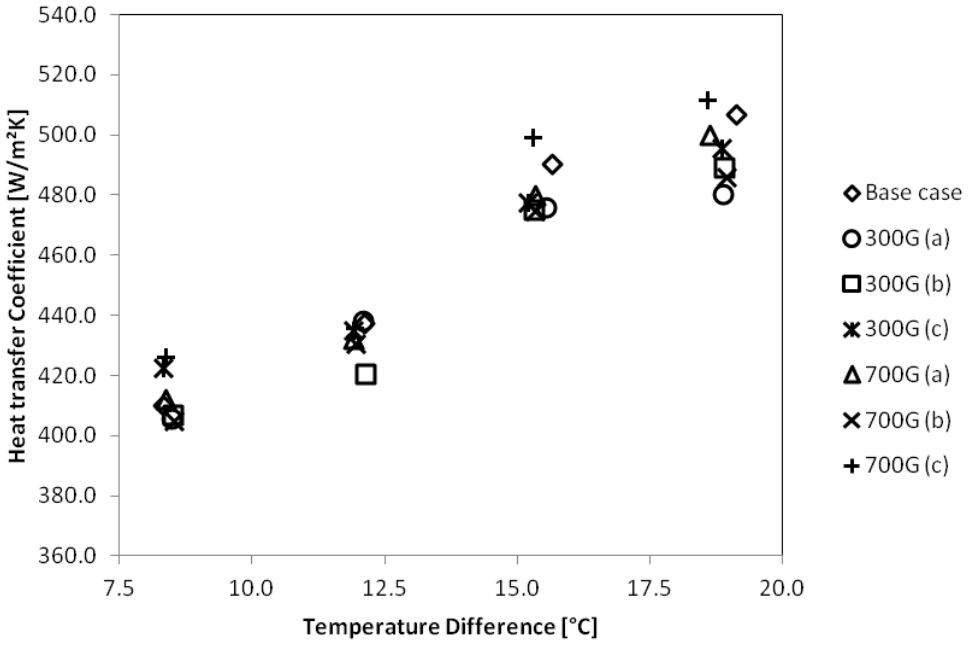

Figure 46: Heat transfer coefficient at the cold wall as a function of the wall temperature difference

Figure 47 and Figure 48 show the Nu as a function of the wall temperature differences for the hot and the cold sides respectively. These results are used to calculate the mean between the hot- and cold-wall Nu. This value is used as the final result to draw a comparison between the different cases.

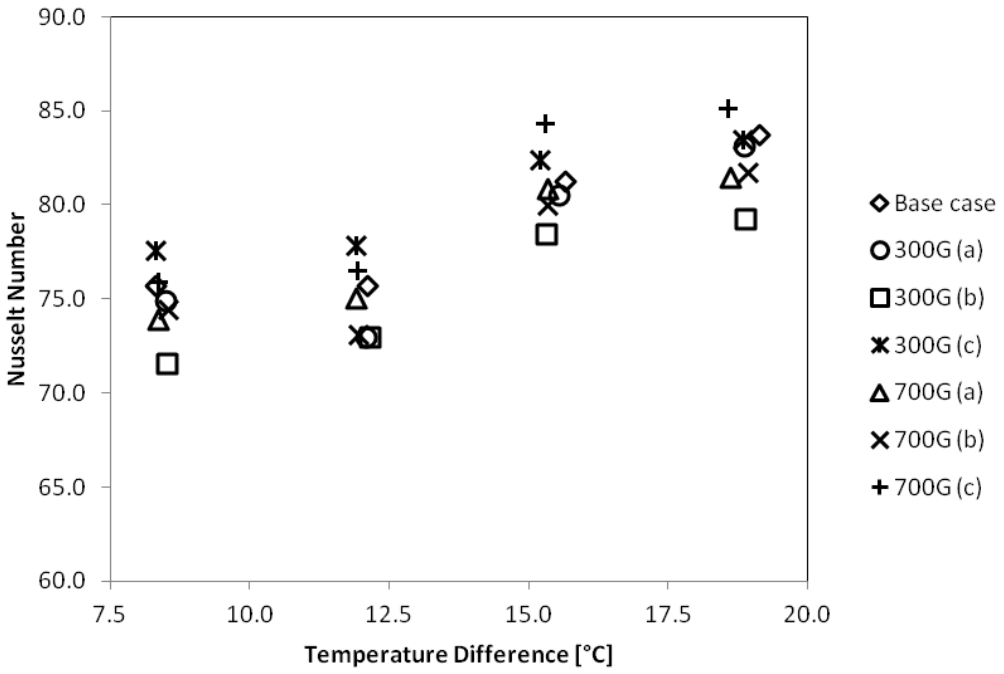

Figure 47: Nusselt number at the hot wall as a function of the wall temperature difference

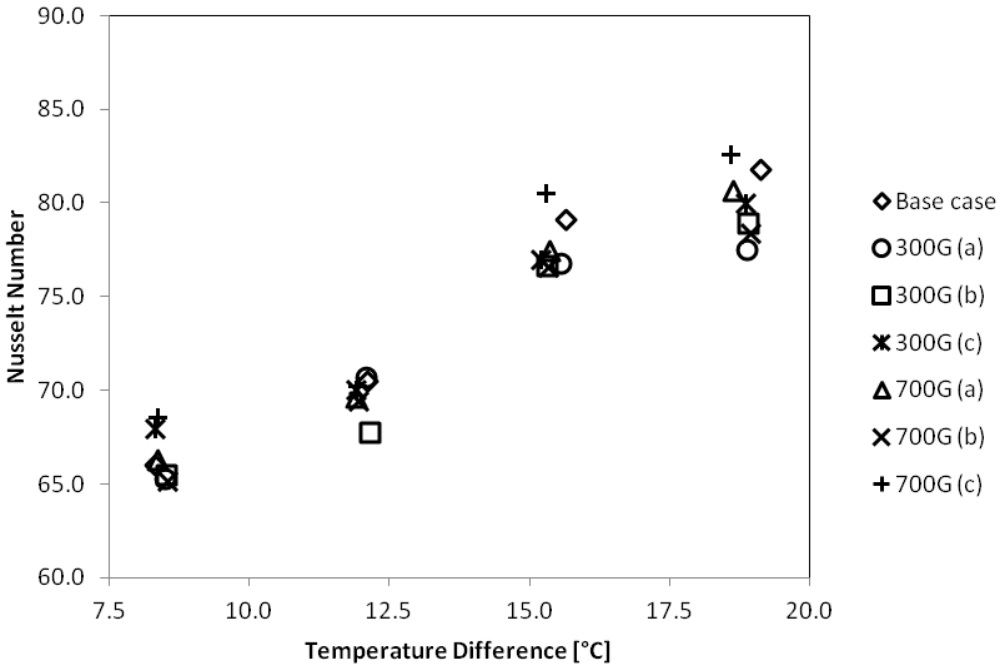

Figure 48: Nusselt number at the cold wall as a function of the wall temperature difference

To summarise the results in this section, two different comparisons are drawn. The first is a comparison between similar magnet configurations with different magnets, and the second is a comparison where the magnets used are kept constant while the configuration changes.

The first set of results can be seen in Figure 49 and Figure 50 where the Nu is compared to the Ra for the 700 G and 300 G magnets respectively. A very definite trend can be seen in both sets of

results. It is clear that the configuration that performs the poorest is configuration (b). For the 300 G magnet, this configuration has a maximum and average deterioration of 4.43% and 3.45% from the base case's Nu respectively. The 700 G magnet performs slightly better, with a maximum and average deterioration of 3.25% and 2.12% respectively.

The next best-performing configuration is configuration (a). The 300 G magnet has a maximum and average deterioration of 2.96% and 1.89% respectively. The 700 G magnet has a maximum and average deterioration of 2.06% and 1.25% respectively.

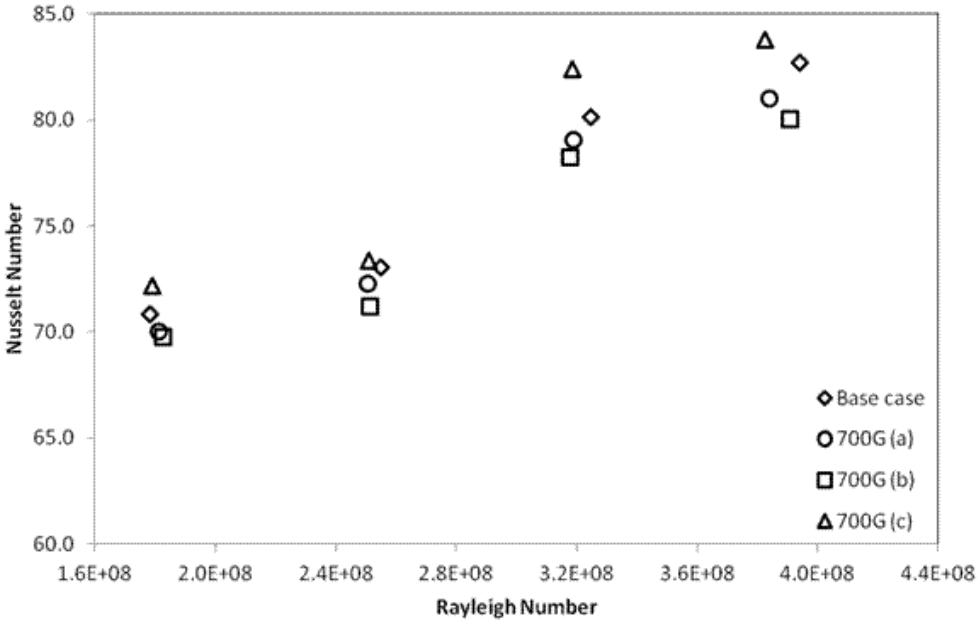

Figure 49: Nusselt number as a function of the Rayleigh number for the 700 G magnet

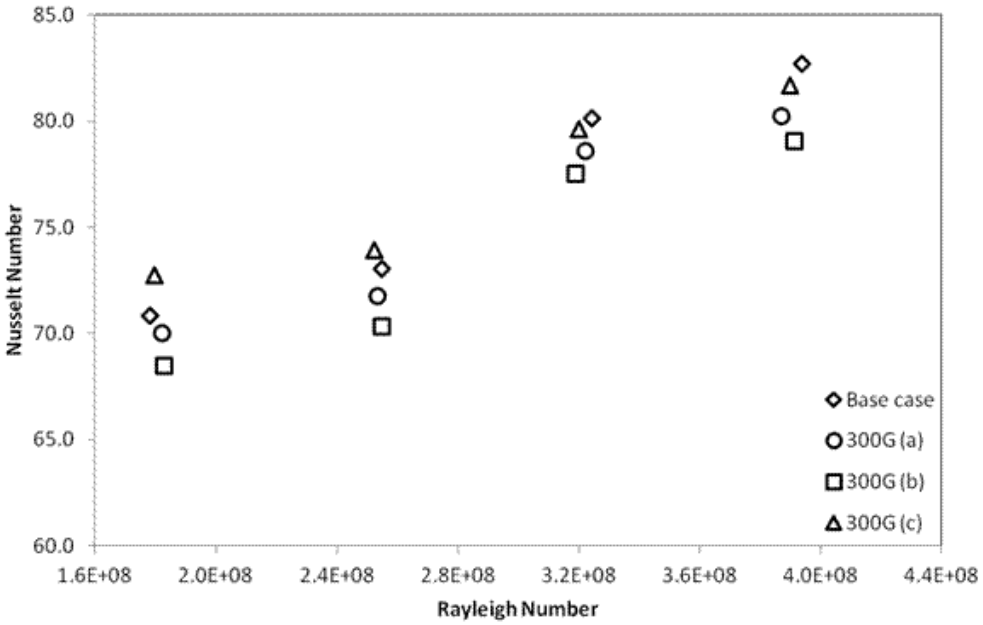

Figure 50: Nusselt number as a function of the Rayleigh number for the 300 G magnet

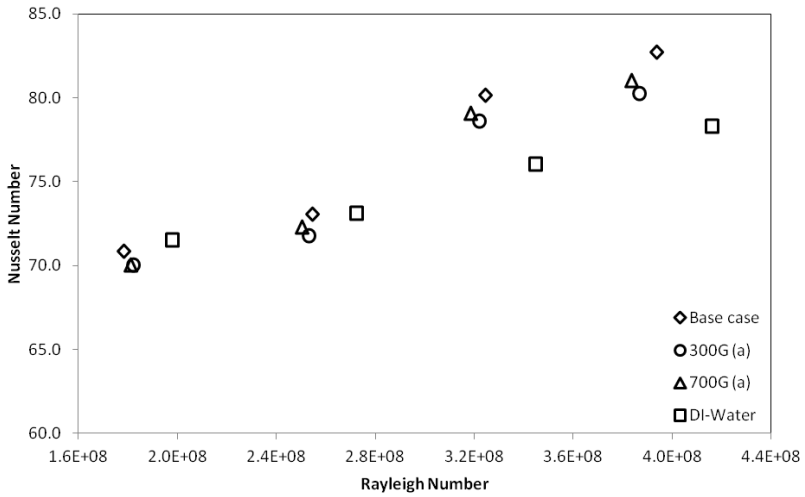

Figure 51: Nusselt number as a function of the Rayleigh number for configuration (a)

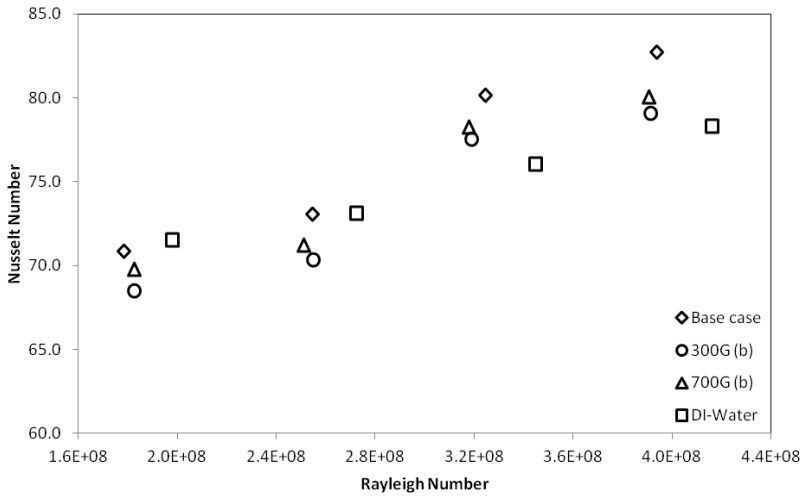

Figure 52: Nusselt number as a function of the Rayleigh number for configuration (b)

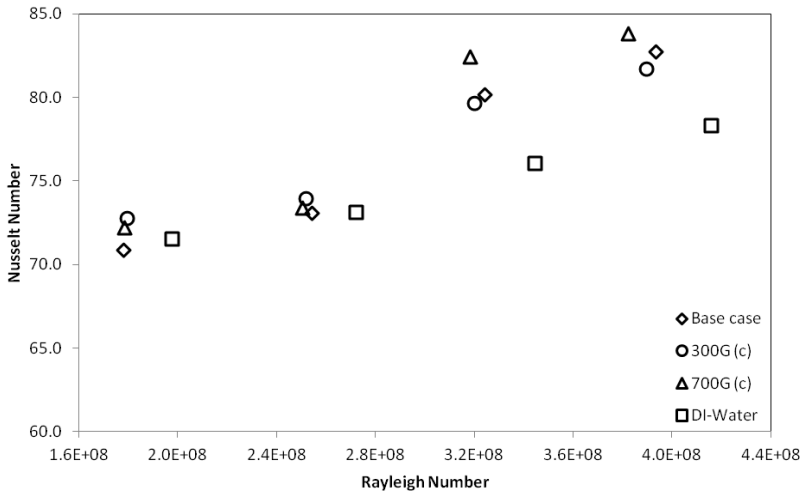

Figure 53: Nusselt number as a function of the Rayleigh number for configuration (c)

Finally, the best-performing configuration is configuration (c). The 300 G magnet performs the best at $Ra = 1.79 \times 10^8$ with an increase of 2.69% of the base case's Nu. The largest deterioration, however, is found to be 1.28% at $Ra = 3.90 \times 10^8$. The average change in Nu is still positive, with an increase of 0.48%. The 700 G magnet has a positive increase for all points. The average increase in Nu is 1.58%, while the maximum increase is given as 2.81% at $Ra = 3.18 \times 10^8$. At a maximum $Ra = 3.82 \times 10^8$, the increase is only 1.32%, pointing to a similar trend of a decrease in performance at a higher Ra.

For all negative cases, the maximum deterioration is found at the largest Ra. All average Nu values were calculated using Equation 4.1.

The final sets of results presented in this section are those of Figure 51 to Figure 53, where the same results are grouped together in terms of the configuration used.

These figures graphically illustrate a result that has already been discussed in the previous results, specifically that the 700 G magnet has a better performance than the 300 G magnet for all cases. It should, however, be noted that these results do not imply that a larger magnetic flux provides a higher Nu. While it is true that the surface magnetic flux is larger, due to the smaller volume of the 700 G magnet, the average magnetic flux inside the cavity is lower due to the smaller volume of fluid sufficiently excited by the 700 G magnetic flux.

4.3 Validation

In order to show that the natural convection setup provided valid results, the heat transfer results for the DI-water obtained in this study is compared to the results of Berkovsky as seen in Equation 1.14 for the same Ra. The comparison can be seen in Figure 54.

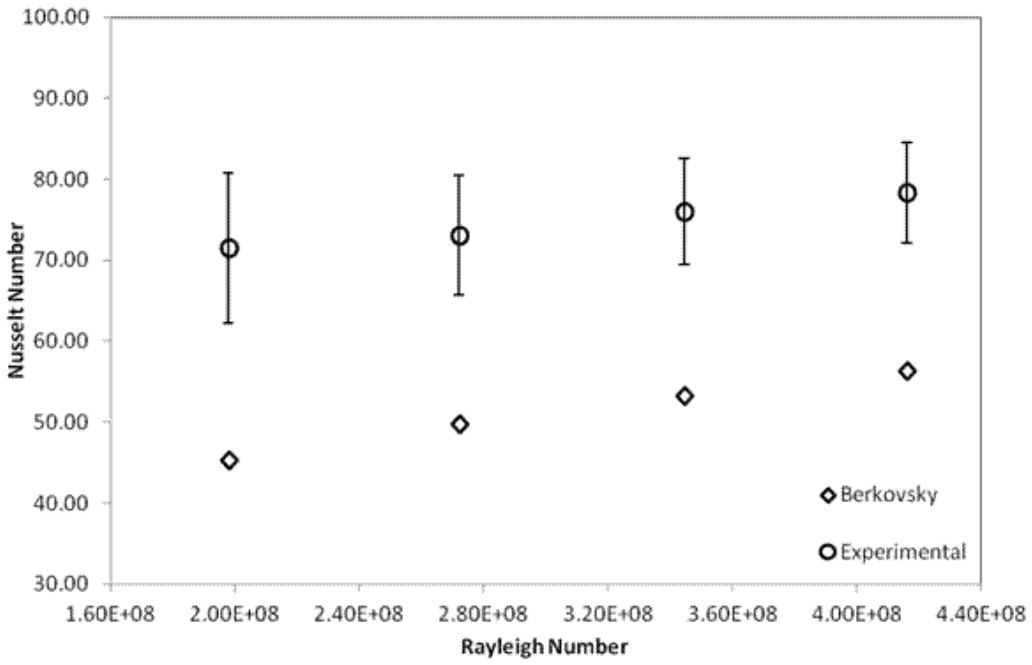

Figure 54: Comparison between experimental results for DI-water and Catton's empirical correlation of Berkovsky results.

From the results it can be seen that the experimental setup provides an overestimates to the results obtained by Berkovsky, however, it can be seen that both results follow a similar trend with the experimental results simply being offset to that found by Berkovsky. For lower Ra, it can be seen that the setup does follow a slightly different trend with the results from literature decreasing more rapidly.

4.4 Conclusion

To summarise the results of this chapter, one should first consider the effects of volume concentration on the heat transfer performance of the fluid. From the results presented, it is clear that there is indeed an optimal volume concentration for a maximum increase in heat transfer. The best-performing fluid throughout all runs is the $\phi = 0.05\%$ nanofluid, while the best-performing nanofluid at the maximum tested Ra is the $\phi = 0.1\%$.

Unfortunately, this shows that the optimal volume concentration is not fixed, but rather that it depends on the operating conditions. This can be explained when considering that the driving force of heat transfer in natural convection systems becomes larger at a higher Ra, allowing the fluid to transport the nanoparticles more effectively, thus allowing the system to make use of the increased thermal conductivity of nanofluids of a higher volume fraction, despite the increased viscosity of the fluid. If this behaviour persists at a Ra significantly higher than the range of interest in this study, it is possible that even a higher volume concentration would perform better.

Moving on to the effect of magnetic fields on the heat transfer performance of the nanofluid, it is noticed that the effects of the magnetic field are not as large as would be expected when considering the tremendous increase in the thermal conductivity and viscosity of nanofluids in the presence of a magnetic field. It should be noted, however, that the increase in the thermophysical properties is due to a magnetic field throughout the whole fluid body, whereas in this study, only a small fluid volume local to the magnets is significantly excited. This being said, it is clear that even the small excitation provided by the magnets influences the heat transfer behaviour of the system to a significant degree.

An interesting behaviour found with most of tested cases was that the use of magnets actually decreased the performance of the nanofluid, with only test case (c) showing any increase in performance for either magnet tested. While it is possible that this is caused by an increase in viscosity, due to the relatively small area significantly influenced by the magnets, it is more likely that the magnets introduced a body force that acts as a damper on the fluid flow.

Considering that case (c) with the 700 G magnet indeed increases performance, compared to the base nanofluid for all cases, it is clear that the use of magnet fields can be used to improve the performance of the nanofluid, albeit with a very specific choice of magnetic field.

Chapter 5: Concluding remarks

The results of the previous chapters are summarised in this final chapter. Remarks are also made about the stability and choice of nanofluids used. The conclusions from the study on the effects of both nanoparticle concentration and magnetic field on the heat transfer of the nanofluid are presented with the intention of discussing the effects of using a magnetic nanofluid, excited by a magnetic field, on the performance of a heat transfer system.

For the purposes of this discussion, a conclusion will be drawn from the presented results, followed by recommendations for future work.

5.1 Summary of findings

The thermophysical properties of the investigated nanofluids show a very similar behaviour to those in other studies. Indeed, the viscosity is found to increase by a considerable factor as the volume concentration increases. When one looks at the behaviour of the thermal conductivity of a similar nanofluid, one can see that the thermal conductivity increases considerably with an increase in volume concentration. This leads to the conclusion that not only for natural convection cases, but also for convection cases, there is an optimum concentration that would yield the maximum heat transfer.

The stability analysis yielded counter-intuitive results. For both the pH adjustment and stabiliser study, it was found that the lower volume fraction cases had a much poorer stability than the higher volume fraction cases. Of course, this is not true indefinitely when one considers the pH adjustment of a higher volume concentration. A possible explanation of this is that, with an increase in particles, the interaction between the charged particles is sufficient to keep the particles suspended. However, this is only a suggestion, and should be confirmed in future studies. This lead to the belief that the stability of a nanofluid also has an optimum concentration, where the positive effects on nanofluid stability caused by particle interaction significantly dominate the fluid-particle interaction. Nanofluids used in natural convection studies present in this work have been shown to have steady thermophysical properties for a duration significantly longer than that of the natural convection tests.

When one considers the natural convection results, it is clear that maximum heat transfer over the range of tested Ra is found at $\phi = 0.05\%$. However, at the maximum Ra, $\phi = 0.1\%$ showed the best performance. The obvious conclusion that can be drawn from this is that the volume concentration that yields the best results is not stationary, but rather a function of the operating conditions. When considering a nanofluid of a higher concentration, it can be seen that it performs significantly poorer than the base fluid, and so by extension even poorer compared to nanofluids of a lower concentration. Since the fluid is only driven by buoyancy effects, the increase in viscosity, as well as the decrease in the thermal expansion coefficient associated with an increase in volume concentration, has a deteriorating effect, which opposes the effect of the increased thermal conductivity, which explains these results.

The effect of exciting the nanofluid via a magnetic field generated by permanent magnets was also shown to have an effect on the heat transfer performance of the system. A definite positive enhancement was shown for one case (700 G (c)), where a weak magnetic flux was used to excite

only the nanofluid close to the hot wall. A higher average flux only at the hot wall (300 G (c)) was shown to have an increase at a lower Ra. However, at a higher Ra, this case showed a decrease in performance as well. All other tested cases showed a negative performance compared to the case with no magnetic field.

From these results, it is clear that enhancement of heat transfer due to natural convection can be obtained by only changing the base fluid to an acceptable nanofluid. Furthermore, if this nanofluid possesses strong magnetic properties, the heat transfer can be enhanced even further, given that the nanofluid is excited correctly by a magnetic field. The negative consequence of this statement relies on the determination of an acceptable nanofluid and magnetic field, as this study does not answer the question on how to predict which nanofluid and the magnetic field will provide this said increase, but rather shows experimentally that such a case exists.

5.2 Recommendations for future work

As is evident from the stability study, even though a sufficient stability was obtained for the required tests, there is clearly room for improvement. For future studies, a premixed nanofluid can be considered as this should not only have a much better stability, but will also ensure better control over the volume fraction and dispersion of the nanoparticles in the nanofluid. Also, as an added benefit, the mixing times will be faster for new nanofluids. An investigation into the effects of the pH adjustment of a nanofluid with stabilisers should also be performed, as this has been found in the literature to provide benefits to the stability of nanofluids as well.

While the viscosity of the nanofluids of interest has been studied and found to be in agreement with other results found in the literature, the thermal conductivity information was obtained from the literature directly. Due to the high sensitivity of the thermophysical properties of nanofluids to a wide range of factors, future work should include a study of the thermal conductivity of nanofluids to be used in testing.

In order to perform accurate magnetohydrodynamic (MHD) simulation, the electrical conductivity of the nanofluid should be studied as well.

The final recommendation that can be made for future work on the study of the thermophysical properties would be to consider determining the effects of a constant magnetic field on the viscosity and thermal conductivity of the nanofluid.

Due to the limitations placed on the allowable volume fraction by the nanofluid stability, it is possible that nanofluids of a lower volume concentration may present even greater enhancement to the heat transfer performance. It, therefore, makes sense that, if a more stable nanofluid is obtained using the suggestion above, nanofluids of a lower volume concentration should also test as a way to bracket the turning point of the heat transfer as a function of volume concentration and focus future research in that area.

Now that this study has shown that an improvement in heat transfer can be obtained, at least for certain magnetic fields, one could improve upon this idea. The first step would be to replace the permanent magnets with electromagnets to allow for easy tuning of the magnetic field, as well as to create transient magnetic fields. These electromagnets should allow the most basic magnetic field to

be analysed, namely a constant magnetic field throughout the cavity. When considering the work done in this study, specifically, in order to quantify the magnetic field and its effect on the magnetic nanofluid, the magnetic field created by the permanent magnets should be determined experimentally and/or numerically.

The work is done in this paper also presents many opportunities for numerical studies. The first tool that may provide insight into the more complex behaviour of nanofluids is a molecular dynamic (MD) simulation. As mentioned in section 5.1, it is uncertain why the nanofluid's stability behaves the way it does. Understanding this behaviour is key to determining not only how to find the most stable nanofluid, but also how to improve this stability even further. The other area where MD can be applied is in determining the effects of a magnetic field on the thermophysical properties of nanofluids.

As with MD simulations, MHD simulations have already been applied to a wide range of nanofluid problems, but they have rarely been applied and compared to experimental work. As this is the case, it is highly recommended that MHD simulations are performed for the cases discussed in this work in order to tune the MHD models to incorporate the complex fluid-particle interactions present in nanofluids.

References

[1] H. Aybar, M. Sharifpur, M. Azizian, M. Mehrabi and J. Meyer, "A review of thermal conductivity models for nanofluids," *Heat Transfer Engineering,* vol. 36, no. 13, p. 1085–1110, 2015.

[2] J. Philip, P. Shima and B. Raj, "Nanofluid with tunable thermal properties," *Applied Physics Letters,* vol. 92, no. 4, 2008.

[3] J. Meyer, S. Adio, M. Sharifpur and P. Nwosu, "The viscosity of nanofluids: A review of the theoretical, empirical, and numerical models," *Heat Transfer Engineering,* vol. 37, no. 5, p. 387–421, 2015.

[4] P. Shima, J. Philip and B. Raj, "Magnetically controllable nanofluid with tunable thermal conductivity and viscosity," *Applied Physics Letters,* vol. 95, no. 13, 2009.

[5] H. O'Hanley, J. Buongiorno, T. McKrell and L. Hu, "Measurement and model validation of nanofluid specific heat capacity with differential scanning calorimetry," *Advances in Mechanical Engineering,* vol. 2012, p. 1–6, 2012.

[6] M. Sharifpur, S. Yousefi and J. Meyer, "A new model for density of nanofluids including nanolayer," *International Communications in Heat and Mass Transfer,* vol. 78, p. 168–174, 2016.

[7] Q. Li, Y. Xuan and J. Wang, "Experimental investigations on transport properties of magnetic fluids," *Experimental Thermal and Fluid Science,* vol. 30, no. 2, p. 109–116, 2005.

[8] M. Alsaady, R. Fu, B. Li, R. Boukhanouf and Y. Yan, "Thermo–physical properties and thermo–magnetic convection of ferrofluid," *Applied Thermal Engineering,* vol. 88, p. 14–21, 2015.

[9] M. Goharkhah, A. Salarian, M. Ashjaee and M. Shahabadi, "Convective heat transfer characteristics of magnetite nanofluid under the influence of constant and alternating magnetic field," *Powder Technology,* vol. 274, p. 258–267, 2015.

[10] M. Zafarani-Moattar and R. Majdan-Cegincara, "Stability, rheological, magnetorheological and volumetric characterizations of polymer based magnetic nanofluids," *Colloid and Polymer Science,* vol. 291, no. 8, p. 1977–1987, 2013.

[11] W. Yu, H. Xie, L. Chen and Y. Li, "Enhancement of thermal conductivity of kerosene–based Fe3O4 nanofluids prepared via phase–transfer method," *Colloids and Surfaces A: Physicochemical and Engineering Aspects,* vol. 355, no. 1–3, p. 109–113, 2010.

[12] R. Hong, S. Zhang, Y. Han, H. Li, J. Ding and Y. Zheng, "Preparation, characterization and application of bilayer surfactant–stabilized ferrofluids," *Powder Technology,* vol. 170, no. 1, p. 1–11, 2006.

[13] B. Bateer, Y. Qu, X. Meng, C. Tian, S. Du, R. Wang, K. Pan and H. Fu, "Preparation and magnetic performance of the magnetic fluid stabilized by bi–surfactant," *Journal of Magnetism and Magnetic Materials,* vol. 332, p. 151–156, 2013.

[14] B. Sun, C. Peng, R. Zuo, D. Yang and H. Li, "Investigation on the flow and convective heat transfer characteristics of nanofluids in the plate heat exchanger," *Experimental Thermal and Fluid Science,* vol. 76, p. 75–86, 2016.

[15] B. Sun, W. Lei and D. Yang, "Flow and convective heat transfer characteristics of Fe2O3–water nanofluids inside copper tubes," *International Communications in Heat and Mass Transfer,* vol. 64, p. 21–28, 2015.

[16] Babita, S. Sharma and S. Gupta, "Preparation and evaluation of stable nanofluids for heat transfer application: A review," *Experimental Thermal and Fluid Science,* vol. 79, p. 202–212, 2016.

[17] X. Li, D. Zhu and X. Wang, "Evaluation on dispersion behavior of the aqueous copper nano–suspensions," *Journal of Colloid and Interface Science,* vol. 310, no. 2, p. 456–463, 2007.

[18] D. Wen and Y. Ding, "Formulation of nanofluids for natural convective heat transfer applications," *International Journal of Heat and Fluid Flow,* vol. 26, no. 6, p. 855–864, 2005.

[19] Y. Çengel and A. Ghajar, Heat and mass transfer, New York, NY: McGraw Hill Higher Education, 2011.

[20] H. Ghodsinezhad, M. Sharifpur and J. Meyer, "Experimental investigation on cavity flow natural convection of Al2O3–water nanofluids," *International Communications in Heat and Mass Transfer,* vol. 76, p. 316–324, 2016.

[21] A. Karimi, M. Goharkhah, M. Ashjaee and M. Shafii, "Thermal conductivity of Fe2O3 and Fe3O4 magnetic nanofluids under the influence of magnetic field," *International Journal of Thermophysics,* vol. 36, no. 10–11, p. 2720–2739, 2015.

[22] R. Azizian, E. Doroodchi and B. Moghtaderi, "Influence of controlled aggregation on thermal conductivity of nanofluids," *Journal of Heat Transfer,* vol. 138, no. 2, 2016.

[23] S. S. Harandi, A. Karimipour, M. Afrand, M. Akbari and A. D'Orazio, "An experimental study on thermal conductivity of F-MWCNTs–Fe3O4/EG hybrid nanofluid: Effects of temperature and concentration," *International Communications in Heat and Mass Transfer,* vol. 76, pp. 171-177, 2016.

[24] E. Ghasemi, A. Mirhabibi and M. Edrissi, "Synthesis and rheological properties of an iron oxide ferrofluid," *Journal of Magnetism and Magnetic Materials,* vol. 320, no. 21, p. 2635–2639, 2008.

[25] S. Odenbach and H. Störk, "Shear dependence of field–induced contributions to the viscosity of magnetic fluids at low shear rates," *Journal of Magnetism and Magnetic Materials,* vol. 183, no.

1–2, p. 188–194, 1998.

[26] L. Sundar, M. Singh and A. Sousa, “Enhanced heat transfer and friction factor of MWCNT–Fe3O4/water hybrid nanofluids,” *International Communications in Heat and Mass Transfer,* vol. 52, p. 73–83, 2014.

[27] M. Sharifpur, N. Tshimanga and J. Meyer, “Parametric Analysis of Effective Thermal Conductivity Models for Nanofluids,” in *ASME 2012 International Mechanical Engineering Congress & Exposition, IMECE 2012*, Houston, Texas, USA., November 9–15, 2012.

[28] M. Ramires, C. Nieto Castro, Y. Nagasaka, A. Nagashima, M. Assael and W. Wakeham, “Standard reference data for the thermal conductivity of water,” *Journal of Physical and Chemical Reference Data,* vol. 24, no. 3, p. 1377–1381, 1995.

[29] H. Patel, T. Sundararajan, T. Pradeep, A. Dasgupta, N. Dasgupta and S. Das, “A micro–convection model for thermal conductivity of nanofluids,” *Pramana – Journal of Physics,* vol. 65, no. 5, p. 863–869, 2005.

Appendix

Appendix A: Thermocouple calibration

The same cavity used in a study by Ghodsinezhad et al. [20] was modified to allow magnets to be placed at the top and bottom of the cavity. In order to do that the cavity was disassembled and only the heat exchanger was used in the reconstruction. New thermocouples were put into the cavity. The same onboard calibration of the data logger/PC was used. This caused the temperature measurements to deviate slightly from the true value.

To control the temperature of the fluid measured by the thermocouples, the thermocouples were placed in a PR20R-30 Polyscience constant thermal bath. The thermal bath's temperature was varied from $3\,℃$ to $60\,℃$ in intervals of $3\,℃$. The thermocouple measurements were compared to the temperature reading given by the thermal bath, which is accurate to 0.005 °C.

The thermocouples were calibrated by fitting a linear model to each set of measurements using linear regression. A thousand measurements were taken at a sampling rate of $1\,\mathrm{kHz}$ for each thermocouple. The average of these values was considered to be the measured value.

With the linear regression taking the form of $T_m = mT_a + c$, with T and T_m being the actual and measured temperature respectively, and m and c being regression constants, the corrected value was calculated as:

$$T = \frac{T_m - c}{m} \tag{A1.1}$$

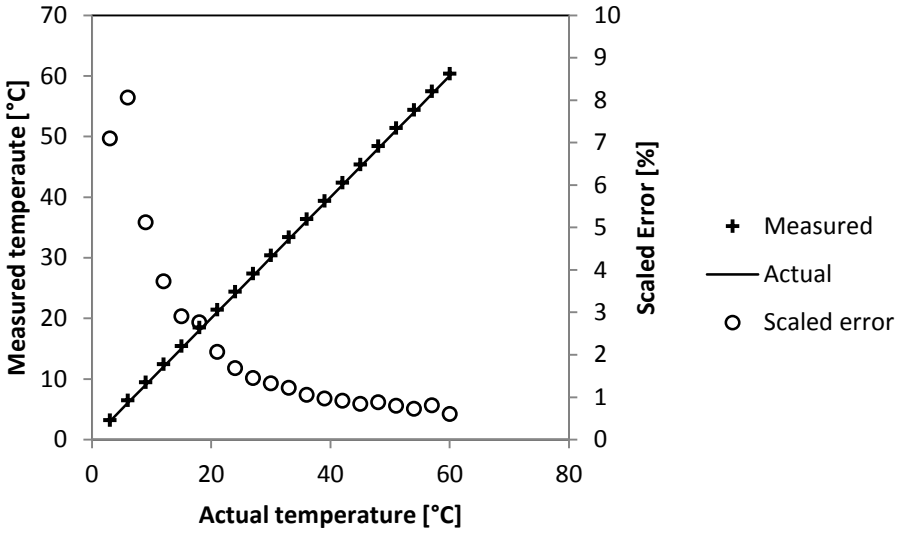

Figure 55: Uncorrected average temperature measurements of all thermocouples

This was done for each thermocouple used. However, to present the results of the calibration, the average results over all the thermocouples are presented against the thermal bath temperature in Figure 55. From the temperature reading, it can be seen that the thermocouples already accurately

measure the actual temperature. The scaled error also follows a very predictable curve, considering that a very constant error is present in all measurements.

The results of the calibration can be seen in Figure 56. It can be seen that the calibration is successful, with the largest scaled error at lower temperatures as expected and a slight error showing itself at $18\ °C$, most likely due to some external influence on the measurement process for that point. The large error at $3\ °C$ is most likely due to the reading being close to the tolerance of the data logging equipment.

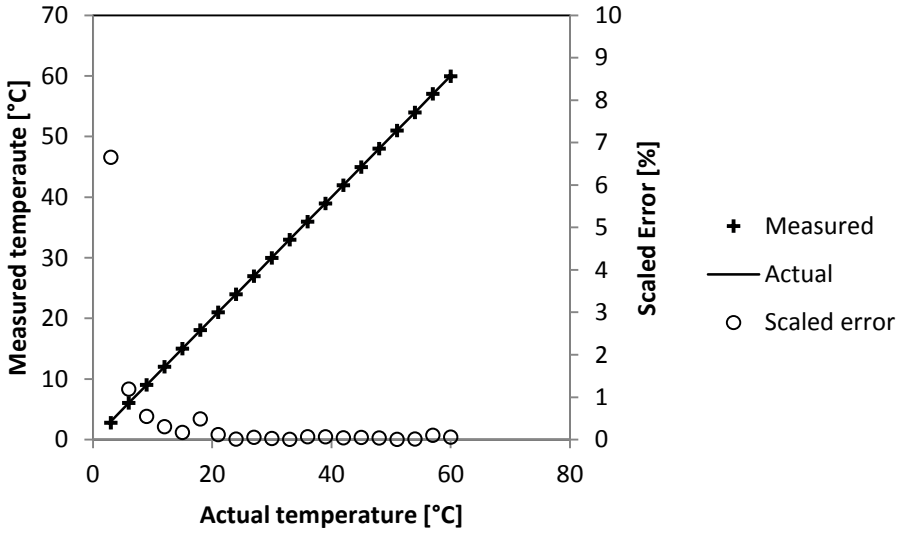

Figure 56: Corrected average temperature measurements of all thermocouples

Before calibration, the maximum error for all thermocouples over all temperature readings was found to be $0.89\ °C$, while the average error was found to be $0.43\ °C$. Again, for all measurements, a maximum error of $0.38\ °C$ and an average error of $0.04\ °C$ was obtained after calibration.

Appendix B: Uncertainty analysis

It is desired to find the uncertainty in the heat transfer coefficient and Nu. This can be calculated using:

$$\delta\dot{Q} = \left(\left(\frac{\partial Q}{\partial \dot{m}}\delta\dot{m}\right)^2 + \left(\frac{\partial Q}{\partial c_{p,nf}}\delta c_{p,nf}\right)^2 + \left(\frac{\partial Q}{\partial \Delta T}\delta\Delta T\right)^2\right)^{\frac{1}{2}} \tag{B2.1}$$

$$\delta h = \left(\left(\frac{\partial h}{\partial \dot{Q}}\delta\dot{Q}\right)^2 + \left(\frac{\partial h}{\partial A}\delta A\right)^2 + \left(\frac{\partial h}{\partial T_h}\delta T_h\right)^2 + \left(\frac{\partial h}{\partial T_c}\delta T_c\right)^2\right)^{\frac{1}{2}} \tag{B2.2}$$

$$\delta Nu = \left(\left(\frac{\partial Nu}{\partial h}\delta h\right)^2 + \left(\frac{\partial Nu}{\partial L_c}\delta L_c\right)^2 + \left(\frac{\partial Nu}{\partial k_{nf}}\delta k_{nf}\right)^2\right)^{\frac{1}{2}} \tag{B2.3}$$

Considering Equation 2.2:

$$\frac{\partial Q}{\partial \dot{m}} = C_p\Delta T, \qquad \frac{\partial Q}{\partial c_{p,nf}} = \dot{m}\Delta T, \qquad \frac{\partial Q}{\partial \Delta T} = \dot{m}C_p \tag{B2.4}$$

Considering Equation 2.4:

$$\begin{aligned} \frac{\partial h}{\partial \dot{Q}} &= \frac{1}{(T_h - T_c)A_s}, & \frac{\partial h}{\partial A} &= \frac{-\dot{Q}}{(T_h - T_c)A_s^2}, \\ \frac{\partial h}{\partial T_h} &= \frac{-\dot{Q}}{(T_h - T_c)^2 A_s}, & \frac{\partial h}{\partial T_c} &= \frac{\dot{Q}}{(T_h - T_c)^2 A_s} \end{aligned} \tag{B2.5}$$

Considering Equation 2.5:

$$\frac{\partial Nu}{\partial h} = \frac{L_c}{k}, \qquad \frac{\partial Nu}{\partial L_c} = \frac{h}{k}, \qquad \frac{\partial Nu}{\partial k_{nf}} = -\frac{hL_c}{{k_{nf}}^2} \tag{B2.6}$$

Substituting equations B2.4 to B2.6 into equations B2.1 to B2.2, the uncertainties are now written as:

$$\delta\dot{Q} = \sqrt{\left(C_p\Delta T\delta\dot{m}\right)^2 + \left(\dot{m}\Delta T\delta c_{p,bf}\right)^2 + \left(\dot{m}C_p\delta\Delta T\right)^2} \tag{B2.7}$$

$$\delta h = \sqrt{\left(\frac{\delta\dot{Q}}{(T_h - T_c)A_s}\right)^2 + \left(\frac{\dot{Q}\delta A}{(T_h - T_c)A_s^2}\right)^2 + \left(\frac{\dot{Q}\delta}{(T_h - T_c)^2 A_s}\right)^2 (T_h + T_c)^2} \tag{B2.8}$$

$$\delta Nu = \sqrt{\left(\frac{L_c\delta h}{k}\right)^2 + \left(\frac{h\delta L_c}{k}\right)^2 + \left(\frac{hL_c}{{k_{nf}}^2}\delta k_{nf}\right)^2} \tag{B2.9}$$

The derived uncertainties are given as:

$$\delta c_{p,bf} = \frac{\partial c_{p,bf}}{\partial T}\delta T_{bulk,hx} \tag{B2.10}$$

$$\delta T_{bulk,hx} = \frac{1}{3}\sqrt{\left(\delta T_{o,1}\right)^2 + \left(\delta T_{o,2}\right)^2 + (\delta T_i)^2} \tag{B2.11}$$

$$\delta\Delta T = \sqrt{\left(\frac{1}{2}\delta T_{o,1}\right)^2 + \left(\frac{1}{2}\delta T_{o,2}\right)^2 + (\delta T_i)^2} \tag{B2.12}$$

$$\delta T_h = \frac{1}{3}\sqrt{\left(\delta T_{h,1}\right)^2 + \left(\delta T_{h,2}\right)^2 + \left(\delta T_{h,3}\right)^2} \tag{B2.13}$$

$$\delta T_c = \frac{1}{3}\sqrt{\left(\delta T_{c,1}\right)^2 + \left(\delta T_{c,2}\right)^2 + \left(\delta T_{c,3}\right)^2} \tag{B2.14}$$

No information was given as to the uncertainty of the thermal conductivity results for the provided model and so the bias of the measurement for the nanofluid is accepted to be the maximum error of the model. The precision is simply given as:

$$\delta k_{nf,i} = \frac{\partial k}{\partial T}\delta T_{bulk} \tag{B2.15}$$

with:

$$\delta T_{bulk} = \frac{1}{3}\sqrt{\left(\delta T_{mid,1}\right)^2 + \left(\delta T_{mid,2}\right)^2 + \left(\delta T_{mid,3}\right)^2} \tag{B2.16}$$

Wall measurements were taken with a vernier accurate to 0.05 mm.

$$\delta A = \sqrt{(H\delta B)^2 + (B\delta H)^2} = 0.05 \times 10^{-3}\sqrt{H^2 + B^2} \tag{B2.17}$$

The uncertainty of the mass flow rate is determined from the uncertainty in the volume flow rate. The error of the flow meter was used as a bias, while the standard deviation of the flow rate measurement for 1 000 measurement points multiplied by the student's t variable for a 95% confidence interval is used as the precision error.

The error of temperature readings requires some more work.

Linear regression analysis takes N measurement pairs $(x_1, y_1), \ldots, (x_n, y_n)$ and fits a linear function to this data of the form $y_p = \hat{m}x_p + \hat{c}$, where the subscript p denotes a predicted value of y at the new value x_p. The constants are obtained as follows:

$$SS_{xx} = \sum_{i=1}^{N}(x_i - \bar{x})^2 \tag{B2.18}$$

$$SS_{xy} = \sum_{i=1}^{N}(x_i - \bar{x})(y_i - \bar{y}) \tag{B2.19}$$

$$\hat{m} = \frac{SS_{xy}}{SS_{xx}} \tag{B2.20}$$

$$\hat{c} = \bar{y} - \hat{m}\bar{x} \tag{B2.21}$$

The unbiased estimator is given as:

$$\hat{\sigma}^2 = \left(\frac{1}{n-2}\right)\sum_{i=1}^{N}(y_i - \hat{y})^2 \tag{B2.22}$$

For a predicted variable y_p, the uncertainty in a can be calculated as:

$$\delta y = \pm t\hat{\sigma}\sqrt{\frac{1}{N} + \frac{1}{M} + \frac{\left(x_p - \bar{x}\right)^2}{SS_{xx}}} \tag{B2.23}$$

where M is the number of measurements at point p given as 1 000. Finally, the uncertainty in x can be determined by:

$$\delta x = \frac{\delta y}{\hat{m}}$$

Applying this to the thermocouples with $y = T_m$ and $x = T_a$ with a desired confidence interval of 95% gives the uncertainty in temperature as:

$$\delta T_i = \pm\frac{t_{0.025,N-2}\hat{\sigma}}{\hat{m}}\sqrt{\frac{1}{N} + \frac{1}{M} + \frac{\left(T_p - \bar{T}\right)^2}{SS_{xx}}} \tag{B2.24}$$

This gives the precision of the thermocouple readings. Since this was calibrated to a temperature controlled to 0.005 ℃, this was used as the bias. The total uncertainty in temperature is:

$$\delta T = \sqrt{\delta T_i^2 + 0.005^2} \tag{B2.25}$$

The range of δT for all temperature readings done lies between 0.05% and 0.3%.

It was found that the uncertainty in the difference between the inlet and the outlet temperatures of the heat exchanger was the highest contributing factor to uncertainty in heat transfer. Due to the much higher flow rate at the cold side, this uncertainty at the cold wall is much higher than at the hot wall. As a result, the uncertainty heat transfer was the dominating factor to uncertainty in the heat transfer coefficient.

Considering that the heat transfer coefficient and Nu for the system are taken as an average between the hot and the cold side, the final uncertainty in the presented results is given as:

$$\delta h = \frac{1}{2}\sqrt{(\delta h_h)^2 + (\delta h_c)^2} \tag{B2.26}$$

$$\delta Nu = \frac{1}{2}\sqrt{(\delta Nu_h)^2 + (\delta Nu_c)^2} \tag{B2.27}$$

For the case with no magnetic field, it was found that the maximum uncertainty in the heat transfer coefficient was 14.41%, with an average uncertainty of 9.65%. The results for the Nu are very similar, with a maximum uncertainty of 14.62% and an average uncertainty of 9.98%. The maximum error was found for the 0.1% volume fraction case with the thermal bath temperatures set to 20 °C to 40 °C.

Similar results were found for the case with a magnetic field. It was found that the maximum uncertainty in the heat transfer coefficient was 13.13% with an average uncertainty of 9.48%. The results for the Nu found a maximum uncertainty of 13.36% and an average uncertainty of 9.81%. The maximum error was found for the 300 G (a) case with the thermal bath temperatures set to 20 °C to 40 °C.

For every tested nanofluid, the maximum uncertainty was found at the lowest temperature difference. As the temperature difference becomes larger, the uncertainty in both the Nu and heat transfer coefficient decreases. At the maximum temperature difference settings, the uncertainty was found to be in a range between 7.17% and 8.65% for the heat transfer coefficient and between 7.58% and 8.99% for the Nu for the cases with no magnetic field, while the uncertainty for the cases with a magnetic field were found to be in a range between 7.03% and 7.84% for the heat transfer coefficient and between 7.45% and 8.22% for the Nu.